3-22-2019

Performance Analysis of Angle of Arrival Algorithms Applied to Radiofrequency Interference Direction Finding

Taylor S. Barber

PERFORMANCE ANALYSIS OF ANGLE OF ARRIVAL ALGORITHMS APPLIED TO RADIOFREQUENCY INTERFERENCE DIRECTION FINDING

THESIS

Taylor S. Barber, 1LT, USAF

AFIT-ENG-MS-19-M-008

DEPARTMENT OF THE AIR FORCE
AIR UNIVERSITY

AIR FORCE INSTITUTE OF TECHNOLOGY

Wright-Patterson Air Force Base, Ohio

AFIT-ENG-MS-19-M-008

PERFORMANCE ANALYSIS OF ANGLE OF ARRIVAL ALGORITHMS APPLIED TO RADIOFREQUENCY INTERFERENCE DIRECTION FINDING

THESIS

Presented to the Faculty

Department of Electrical and Computer Engineering

Graduate School of Engineering and Management

Air Force Institute of Technology

Air University

Air Education and Training Command

In Partial Fulfillment of the Requirements for the

Degree of Master of Science in Digital Engineering

Taylor S. Barber, BS

1st Lieutenant, USAF

March 2019

AFIT-ENG-MS-19-M-008

PERFORMANCE ANALYSIS OF ANGLE OF ARRIVAL ALGORITHMS APPLIED TO RADIOFREQUENCY INTERFERENCE DIRECTION FINDING

Taylor S. Barber, BS

1st Lieutenant, USAF

Committee Membership:

Dr. Sanjeev Gunawardena
Chair

Dr. John Raquet
Member

Dr. Phillip Corbell
Member

AFIT-ENG-MS-19-M-008

Abstract

Radiofrequency (RF) interference threatens the functionality of systems that increasingly underpin the daily function of modern society. In recent years there have been multiple incidents of intentional RF spectrum denial using terrestrial interference sources. Because RF based systems are used in safety-of-life applications in both military and civilian contexts, there is need for systems that can quickly locate these interference sources. In order to meet this need, the Air Force Research Laboratory Weapons Directorate is sponsoring the following research to support systems that will be able to quickly geolocate RF interferers using passive angle-of-arrival estimation to triangulate interference sources.

This research studies the performance of angle-of arrival (AoA) estimation algorithms for an existing uniform linear antenna array. Four algorithms are presented, they are phase-shift beamforming, Capon or Minimum Variance Distortionless Response (MVDR) beamforming, the Multiple Signal Identification and Classification (MUSIC) algorithm, and one instantiation of a Maximum Likelihood Estimation (MLE) algorithm. A modeling and simulation environment using MATLAB™ is developed and the performance of each algorithm is simulated as implemented on a uniform linear array. Performance is characterized under various non-ideal conditions.

Based on the results of the performance study and a computational complexity analysis of the four algorithms, a hybridized AoA estimation algorithm is recommended as an optimal solution for the given sensor and mission.

Acknowledgments

First, I would like to thank to my wife for her loving support and patience. She has faithfully supported me not only through this thesis but through our life together; enabling every achievement, supporting me through every trial.

Thank you to my mother who gave me life – and gave me a life.

Thank you to my advisor; your knowledge, guidance, flexibility and support have made this thesis possible. You have improved this thesis as a paper and you have improved me as an engineer in ways that will never be fully appreciated.

Thank you to my coworkers at the AFRL sensors directorate for your support over the last year and for allowing me to balance our mission against this one.

Thank you to my committee members, your lifelong commitment to the pursuit of knowledge have made this research possible.

This research was sponsored by the Air Force Research Laboratory - Weapons Directorate at Eglin AFB, Florida.

Taylor S. Barber, 1Lt, USAF

Table of Contents

Page

List of Figures

Page

List of Tables

Page

List of Abbreviations

ADC	Analog to Digital Converter
AoA	Angle of Arrival
CRB	the Cramer-Rao bound
FOR	Field of Regard
IF	Intermediate Frequiency
M&S	Modeling and Simulation
MLE	the Maximum Likelihood Estimation Algorithm
MUSIC	the Multiple Signal Classification and Identification Algorithm
MVDR	Minimum Variance Distortionless Response
PSBF	Phase-Shift Beamformer
RF	Radio Frequency
SNR	A ratio of signal power to noise power
TOA	Time-of-Arrival
ULA	Uniform Linear Array

List of Symbols

ϵ	An error term
ϕ	An arbitrary phase shift (radians)
π	pi ≈ 3.14159265359
Σ	A diagonal matrix where the entries are the eigenvalues of a matrix
τ	Time delay (seconds)
τ_N	Time delay (seconds) at the Nth element of a ULA relative to the first element.
$A\Theta$	An $N \times (N\text{-}1)$ matrix where the columns are values of $A(\theta)$
$A(\theta)$	The array manifold
$\dot{A}(\theta)$	The derivative of $A(\theta)$ with respect to θ
$abs()$	The absolute value function
b	Samples of an N-element ULA
C	An estimated covariance matrix
c	The speed of light $= 299{,}792{,}458$ meters/second
d	Element spacing in a ULA
d_n	Distant of the n_thelement from the center of a ULA
L	The number of samples in a block used to estimate AoA
M	Number of transmission sources in the FOR
$\frac{M}{D}$	A ratio of multi-path signal power to direct path signal power
N	Number of receive elements in a ULA
$P(\theta)$	Power as a function of angle
$P_{Capon}(\theta)$	The output of the Capon algorithm as a function of AoA

$P_{MLE}(\Theta)$	The output of the MLE algorithm as a function of AoA estimates
$P_{MUSIC}(\theta)$	The output of the MUSIC algorithm as a function of AoA
$P_{PSBF}(\theta)$	The output of the PSBF algorithm as a function of AoA
f_{center}	Center frequency of a bandpass filter
f_{corner}	Corner or cutoff frequency of a filter
f_c	Center frequency = 1575 MHz
f_{sample}	Sample freuqency of an ADC
M&S	Modeling and Simulation
$[S_{Array}(t)]$	An $[N \times 1]$ vector containing the measured RF signals of a plane wave incident on an N-element ULA at a time= t.
$[S_{sampled}(t)]$	An $[N \times 1]$ vector containing the sampled signals of an N-element ULA at a time t
$s_N(t)$	Signal measured at the N_th element of a ULA at a time = t
SVD()	The singular value decomposition
t	time (seconds)
times()	The point-wise multiplication function
t_{sample}	ADC sampling period $= 1/f\_sample$
U	The left-eigenvectors of a matrix
U_{signal}	The eigenvectors that represent the signal suspace
U_{noise}	The eigenvectors that represent the noise subspace
V	The right eigenvectors of a matrix
X_{sample}	A $[N \times L]$ matrix containing block complex signal samples

PERFORMANCE ANALYSIS OF ANGLE-OF-ARRIVAL ALGORITHMS APPLIED TO RADIOFREQUENCY INTERFERENCE DIRECTION FINDING

I. Introduction

Angle-of-Arrival (AoA) measurement of radiofrequency (RF) signal sources has many applications that include geolocation of interference sources, generation of jamming strobes, track-on-jamming applications for weapons, optimization of smart antennas in communication networks, and passive target tracking [1] [2] [3]. This thesis focuses on azimuthal AoA estimation to enable geolocation of interference sources; however, the AoA measurement techniques and algorithms studied in this thesis are relevant and applicable to the full symphony of AoA applications.

RF systems serve the modern world through a broad array of applications including radar, navigation, internet connectivity and other communications networks. In the future self-driving cars and high speed wireless 5G networks will almost certainly increase our dependency on RF systems for everyday productivity as well as safety of life applications. The successful proliferation of RF systems is undermined by their fragility. Because RF systems are almost always constrained by the power available to them and their transmit powers are carefully regulated by bodies such as the Feder Communications Commission [4], many RF systems can be denied through relatively accessible low-power interference systems [5] [6] [7] [8]. Given the importance of RF systems it is vitally important to protect the availability of the electromagnetic spectrum. One method to protect critical RF systems is the prompt detection and attribution of interferers using AoA-based geolocation.

This thesis studies the capability of AoA algorithms to detect RF interferers and determine their AoA using a uniform linear array (ULA). This thesis is organized as follows:

- Section II develops the concept of geolocation of interference sources using AoA, and reviews the foundational theory behind phase-based AoA estimation.
- Section III explains the modeling and simulation (M&S) environment used in this thesis, presents the four AoA algorithms that are studied, and compares the computational complexity of each algorithm.
- Section IV explains the experiments and presents the results of this study.
- Section V ranks the performance of each technique in each test, briefly comments on the most significant findings, presents a hybridized algorithm tailored to the antenna hardware, and recommends AoA algorithms that are best suited for the detection of RF interferers in specific applications.

II. Background

One method for locating radiofrequency (RF) interferers is geolocation based on measuring the angle-of-arrival (AoA) of the interference sources. AoA-based geolocation uses multiple sensors to generate lines of bearing from known sensor locations to the unknown location of the interference source. These lines of bearing intersect at the location of an interference source. This thesis focuses on direction finding in azimuth only. However, all of the techniques studied in this effort can be extended to elevation given the appropriate sensors. Figure 1 shows a simple example where two AoA sensors generate AoA measurements, θ_1 and θ_2, that are used to triangulate a single interference source.

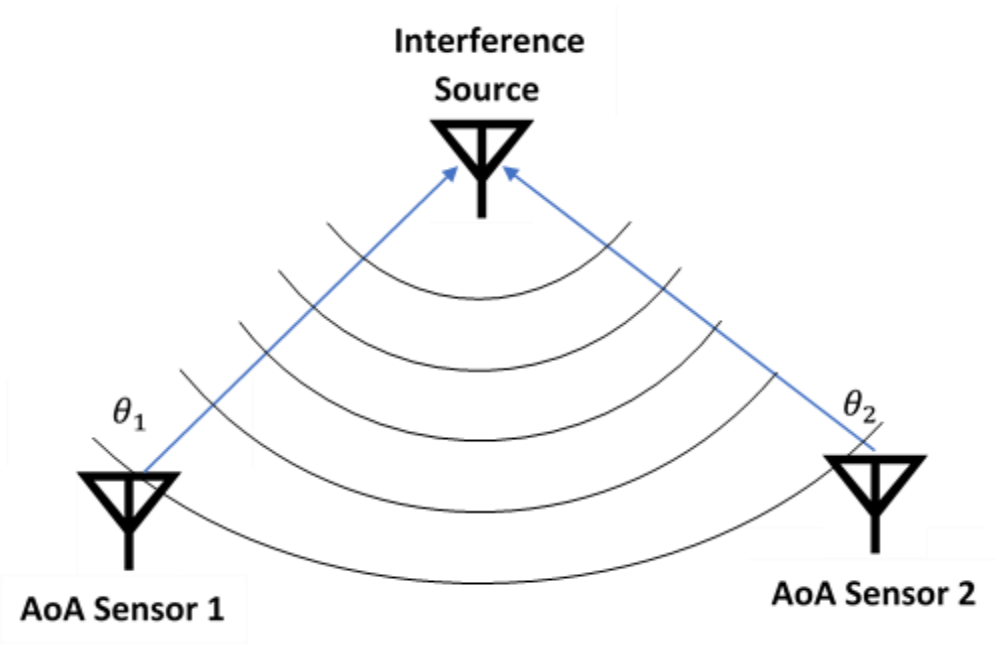

Figure 1. Interference Source Triangulated by Two AoA Sensors

To accurately locate the interference source, precise measurement of AoA at each sensor is critical. For this effort the AoA is measured using a uniform linear array (ULA). A ULA is an antenna that is composed of multiple elements that are uniformly spaced at a known distance from one another. The foundational concepts behind ULA-based AoA estimation are provided in Section 2.1.

2.1 Uniform Linear Array-based Angle of Arrival Estimation

Classical array-based AoA methods are the straightforward applications of foundational antenna array concepts such as beam steering and null steering to detect energy sources in the environment [9]. More recently subspace or “super-resolution” methods have improved on these classical methods by capitalizing on digital system architectures and advanced signal processing [10].

Within this effort, four array-based AoA algorithms are employed:

- The Phase-shift Beamformer (PSBF), which is a straightforward application of array beam steering to the AoA problem.
- The Capon or Minimum Variance Distortionless Response (MVDR) beamformer, which measures the environment by sweeping a destructive interference pattern across the field of regard and measuring the decrease in signal level.
- The Multiple Signal Classification (MUSIC) algorithm, which is a subspace technique based on deconstructing the field of regard into an orthonormal eigenbasis, separating the noise subspace from the signal subspace, and sweeping these enhanced orthogonal nulls across the field of regard.
- The Maximum Likelihood Estimation (MLE) algorithm, which for an N-element array will iteratively search the field of regard with *N-1* beams in an attempt to maximize the amount of energy received by the sensor.

In Section 3.2 each algorithm is briefly derived and in Section 3.3 their computational costs are compared.

When an interference source is present in the far field, a plane wave is incident on the ULA. Figure 2 depicts a six element ULA with elements spaced a distance d apart and a planewave with AoA of θ.

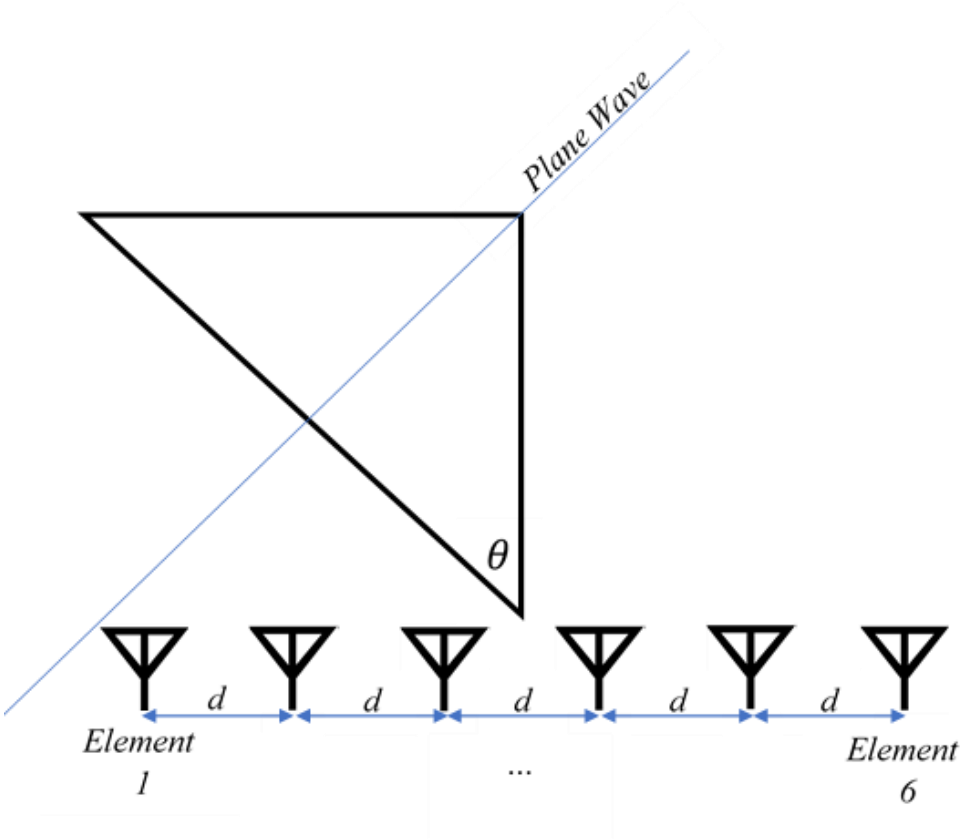

Figure 2. Plane Wave Incident on a Six Element ULA

Let the planewave in Figure 2 be a simple tone with frequency $f_c = 1.575$ GHz and amplitude A. Then the signal is described in (1) where ϕ is some random incident phase with respect to Element 1.

$$s(t) = \frac{A}{\sqrt{(2)}} cos(2\pi f_c t + \phi) \quad (1)$$

Next, consider the time of arrival of the plane wave at the elements of the ULA pictured in Figure 2. Let the time of arrival at element one be zero; then the time of arrival at the N_{th} element, τ_N , is given by (2) where c is the speed of light and θ is the AoA.

$$\tau_N = \frac{d\sin(\theta)(N-1)}{\mathrm{c}} \tag{2}$$

Recalling the signal in (1), and combining with (2) gives the signal received at the N_{th} element, $s_N(t)$ according to (3).

$$s_N(t) = \frac{A}{\sqrt{(2)}} cos(2\pi f_c(t-\tau_N)+\phi) \tag{3}$$

Considering the signal at each element and arranging them in an $[N \times 1]$ matrix gives the array response at RF as shown in (4).

$$[S_{Array}(t)] = \begin{bmatrix} \frac{A}{\sqrt{(2)}} cos(2\pi f_c t+\phi) \\ \frac{A}{\sqrt{(2)}} cos(2\pi f_c(t-\tau_2)+\phi) \\ \dots \\ \frac{A}{\sqrt{(2)}} cos(2\pi f_c(t-\tau_N)+\phi) \end{bmatrix} \tag{4}$$

To go any further we must define a receiver architecture for the sensor. For this effort the parameters of the simulation are set to be consistent with the antenna hardware that the research supports. The receive architecture uses a single down-conversion step with a mixing frequency of 1.565 GHz and an analog to digital converter (ADC) with a 65 MHz sampling rate. The band of interest is 1.575 ± .010 GHz; The number of samples is 1024; the sampling rate is 65 MHz; the intermediate frequency (IF) is 10 MHz; and each AoA sensor is a ULA with *N=6* antenna elements that are spaced 94 mm apart. The hardware uses a block processing method, thus the length of real-time data processed for each AoA

solution is $\frac{1024\ samples}{65\ MHz} = 15.75\ \mu s$. Figure 3 illustrates the modeled ULA, and Figure 4 shows the receiver architecture.

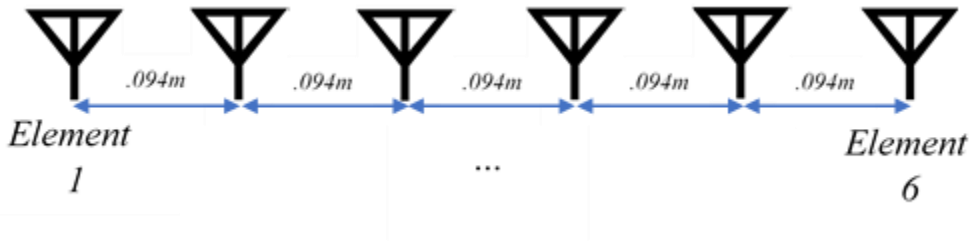

Figure 3. 6-Element ULA with 94 mm Spacing.

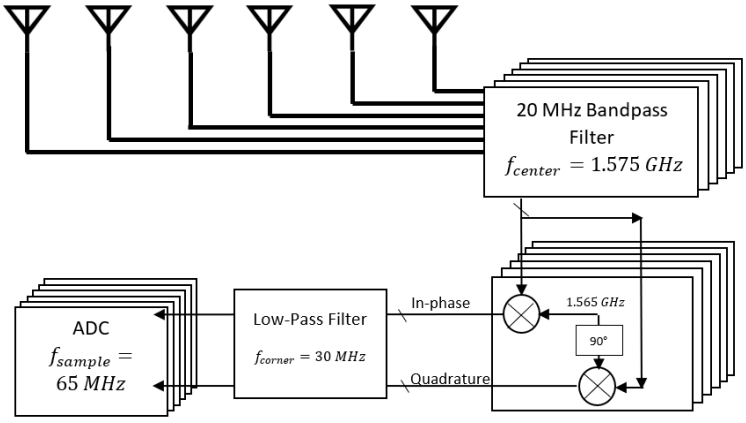

Figure 4. Array Receiver Architecture

After down-conversion let $\phi = 0$ and $t = 0$, then the signal sampled from each element is given by (5).

$$[S_{sampled}(t)] = \begin{bmatrix} Ae^{(0)} \\ Ae^{(i2\pi f_{L1}\tau_2)} \\ \dots \\ Ae^{(i2\pi f_{L1}\tau_N)} \end{bmatrix} \quad (5)$$

Finally, if we let the signal amplitude equal unity, and recall (2) to express the time delays across the array as a function of the AoA of the plane wave, θ from Figure 2, we derive the ULA's response to a unit amplitude plane-wave as a function of the AoA of the wave; this is the calculated array manifold, $A(\theta)$.

$$A(\theta) = \begin{bmatrix} e^{(0)} \\ e^{\left(\frac{i2\pi f_C d sin(\theta)}{c}\right)} \\ \dots \\ e^{\left(\frac{i2\pi f_C d(N-1)\sin(\theta)}{c}\right)} \end{bmatrix} \tag{6}$$

Often is it convenient to define the array manifold relative to the physical center of the array yielding (7) where d_n is the distance of the n_{th} element from the geometric center of the array.

$$A(\theta) = \begin{bmatrix} e^{\left(\frac{i2\pi f_C d_1 sin(\theta)}{c}\right)} \\ e^{\left(\frac{i2\pi f_C d_2 sin(\theta)}{c}\right)} \\ \dots \\ e^{\left(\frac{i2\pi f_C d_N \sin(\theta)}{c}\right)} \end{bmatrix} \tag{7}$$

All of the algorithms studied in this effort use this calculated ULA manifold as hypotheses for the AoA of incoming signals and measure the AoA by determining the commonality between the measured signal at the ULA and this expected array response.

2.2 AoA Estimation Background

Many different methods of establishing AoA have been developed, this section briefly describes the most prevalent algorithms in each class of AoA estimation techniques. The techniques can be broadly classified into four main categories:

- Physical Antenna Rotation
- Beamforming Methods
- Subspace Methods
- Maximum Likelihood Methods

The first attempts at measuring AoA involved exploitation of directional antennas, most commonly relying on physical rotation of a directional, high-gain antenna to register an increase in power when pointed at a signal source [11]. Advances on this concept included monopulse direction finding which uses multiple antenna elements to improve on the conventional approach by comparing the phase response and the amplitude sum and difference measurements of identical elements. The exact time of invention for monopulse direction finding is unknown, but it is believed to have been developed sometime before or during World War II. Monopulse direction finding is sometimes still used but its effectiveness has remained reliant on physical rotation of the antenna over the field of view thus limiting its effectiveness in AoA applications [12].

The advent of phased array radars made direction finding based on beam steering from a fixed antenna a possibility. Because the beams could be steered electronically, array-based sensing can be quickly swept over the field of view by adjusting the phase-shifts across the array. Beamforming using an array can correctly be interpreted as a spatial realization

of classic Fourier-based spectral analysis [3]. More recently software defined radios have enabled simultaneous beamforming in many directions with resolution limited only by computational burden. Two methods of beamforming are most often used for AoA estimation they are: the conventional phase-shift (or Bartlett) beamformer (PSBF), which maximizes the energy from the sum of the array elements at a given AoA, and the Capon or minimum variance distortionless response (MVDR) beamformer [9] which minimizes the energy from the sum of the array elements at a given AoA. As with Fourier spectral analysis there is an infinite number of variations on these basic themes which can improve some performance criteria at the expense of others [13] [14]. Beamforming performance relies heavily on the physical footprint of the antenna and the number of elements in the antenna array. For example, the PSBF method is dependent on the size of the array to produce narrow beams, in practice antenna must be several beamwidths long to achieve a sufficient angular resolution, additionally the elements of the array must be spaced no farther apart than $\frac{\lambda}{2}$ to avoid the grating lobes, which are the spatial analog to aliasing. As a result, the desired angular resolution of the AoA system is a direct result of antenna size and the number of elements. Thus, performance is directly tied to the size and cost of the system.

The most commonly used improvement to beamforming methods are subspace methods, often used subspace methods include Multiple Signal Identification and Classification (MUSIC) and Estimation of Signal Parameters via Rotational Invariance Techniques (ESPIRIT) [15] [10]. Designed for use on uniform linear arrays (ULAs), these techniques rely on decomposition of the signal environment into a covariance matrix. Subspace techniques have been found to have asymptotically efficient performance when the

number of samples is large [16]. The immediate improvement offered by subspace methods is very fine angular resolution. For this reason, subspace methods are often referred to as “super-resolution” techniques. Additionally, they offer some decoupling of the algorithm performance from the size of the array. For example, MUSIC does not require large antennas, in practice MUSIC performance is tied more closely to calibration of the array manifold than the absolute size of the antenna, enabling fine angular resolution from smaller, potentially less expensive apertures.

The primary drawback to subspace methods is that they require a relatively large number of samples and a sufficient signal to noise ratio (SNR) to realize very fine angular resolutions. When the best-possible performance is required with limited sampling information or low SNR precludes the use of subspace methods maximum likelihood estimation (MLE), methods may be used. MLE involves iteratively search through the data to find the most likely solutions. While exhaustive MLE methods have been shown to be the most accurate AoA estimation method they are not commonly used due to the relatively restricted conditions where they offer benefit over subspace methods and because of their increased computational burden [16].

2.3 The Cramer-Rao Lower Bound on AoA Estimation Errors

The well-known Cramer-Rao bound (CRB), given in (8), has established the theoretical lower bound for the variance of AoA errors given a specific antenna, a number of samples, and a SNR [16] [17] [18]. The CRB applied to the AoA problem is given in (9) where L is the number of samples processed in a block by the algorithm, SNR is the linear ratio of

signal to noise power for each of the samples, $A(\theta)$ is the array manifold given in (7), and $\dot{A}(\theta)$is the derivative of the array manifold with respect to θ.

$$CRB = \frac{\frac{1}{L\,SNR}+|A(\theta)|^2}{2L\,SNR\,|A(\theta)|^2\,\left|\dot{A}(\theta)\right|^2} \tag{8}$$

The CRB is commonly simplified for the case where $L\,SNR \gg 1$, yielding (9).

$$CRB \approx \frac{1}{2\,L\,SNR\,\left|\dot{A}(\theta)\right|^2} \tag{9}$$

The value for $\left|\dot{A}(\theta)\right|^2$ for the N-element ULA with array manifold described by (7) is given in (10).

$$\left|\dot{A}(\theta)\right|^2 = \frac{4\pi^2 f_{L1}^2 \cos^2(\theta)\,\sum_{n=1}^{N}(d_n)^2}{c^2} \tag{10}$$

Applying (10) to (9) yields the commonly used estimation of the CRB for an N-element ULA.

$$CRB \approx \frac{c^2}{8\pi^2 L\,SNR\,f_{L1}^2 \cos^2(\theta)\,\sum_{n=1}^{N}(d_n)^2} \tag{11}$$

2.4 AoA Performance Analysis

Today it is commonly suggested that sub-degree angular resolution of interference sources is achievable in real world applications [19] [20] [21] [22], and indeed the CRB seems indicate, provided sufficient samples or SNR, that infinitely precise AoA estimation accuracy is achievable. However, it is important to note that the CRB is a theoretical lower bound on error levels and not necessarily a prediction of performance.

The performance of AoA estimation algorithms in real world systems is a complex topic, and choosing an algorithmic approach must be done carefully. The computational complexity and the performance characteristics of AoA estimation algorithms varies depending on the environment and hardware used. There exists a substantial body of work to characterize the performance of AoA estimators, particularly MUSIC and MLE [16] [23] [24] [25]. It has been noted that published literature that compares algorithm performance in challenging environments is scarce [16], and that in some cases the performance of subspace algorithms may be overstated. There is some body of work that directly compares, for a common set of hardware, the performance of subspace and beamforming techniques [26] [27] [28]. However, such studies are limited in scope with regard to the hardware considered and the error sources modeled.

This research examines the limitations of array-based AoA algorithm performance and the degradation of performance due to non-ideal, real-world considerations for an existing ULA. Specific sources of error studied in this thesis include:

- Cluttered signal environments
- Wideband signals
- Closely spaced signal sources

- Spatially-diverse, phase-coherent sources
- Antenna manufacturing errors
- Phase calibration errors
- Low SNR
- Strong multipath interferers
- Algorithmic limitations to instantaneous dynamic range

By considering algorithm performance in the presence of each of these errors, more informed decisions can be made for the development of AoA systems and realistic performance goals can be set.

III. Methodology

The investigative method of this research is primarily software simulation. When available, data collections using the physical equipment shown in Section II are injected into the simulation to validate the simulation environment.

To study angle-of-arrival (AoA) estimation algorithm performance, a novel simulation environment is developed using MATLAB™. This simulation environment uses continuous-time signal generation models and a first-order physics engine to simulate signal and antenna interaction in three-dimensional space and time.

Given the location and sampling times of each receive antenna, as well as the location of each signal source, the simulator generates the RF signals from each source received by the antenna. After the RF samples are generated, each antenna's receive chain is modeled from the antenna through frequency down-conversion, filtering, and signal digitization. After digitization, each AoA algorithm operates on a common data set and the results are reported.

The remainder of the section is organized as follows: Section 3.1 provides an explanation of the modeling and simulation environment, Section 3.2 describes four AoA estimation algorithms, and Section 3.3 briefly compares the computational complexity of each algorithm.

3.1 Simulation Environment Methodology

To study the performance of AoA algorithms, a modeling and simulation (M&S) environment is developed. This section describes this environment and details the specific instantiation of the environment to support AoA algorithm trade studies.

3.1.1 *General*

To simulate the AoA algorithms it is necessary to simulate electromagnetic waves. All of the AoA methods studied ultimately rely on using relative phase differences between the elements of a uniform linear array (ULA). Therefore, it is necessary simulate amplitude and phase information of all signals in the environment and to model a radiofrequency (RF) receiver including signal reception, mixing, filtering and digitization of the signals prior to presenting the measured information to an AoA algorithm. The simulator developed for this effort fulfills all of the stated goals; however, it should be noted that it does not take into effect various coupling effects between antenna elements or other second-order phenomena that would be present in a physical system.

3.1.2 *Antenna Definition*

Each antenna is defined according to its role in the simulation, these roles are:

- Transmission sources
- Reception antennas
- Multipath sources

Antennas in the simulation environment are treated as ideal isotropic sources and receivers. Every antenna is declared as a point in three-dimensional space - the antenna phase center. For example, the antenna from Figure 4 is modeled by defining six receive antennas along a straight line and that are spaced 94 mm apart.

Additional parameters are defined according to the antenna's role in the simulation. Transmission antennas are specified with a signal amplitude and a complex signal generation function that is continuous for all time. Every signal generation function must

use time as an input and output a complex signal at an RF frequency. For example, (12) shows a signal generation function, [S], for a simple tone with amplitude A, a center frequency, f_c, and an input timing vector [T] that represents the instants in time where the signal is sampled. If the simulation uses L samples, then [T] and [S] will be [L×1] vectors.

$$[S] = Ae^{i2\pi f_c[T]} \tag{12}$$

Multipath sources are modeled as a static transmission source located at the point where the incident signal will reflect. A power modulation factor and a fixed, randomly generated phase shift are also defined for a multipath source. The multipath source inherits the signal generation function of its incident source. Equation (13) gives the signal generation function of a multipath source that is reflecting from the same signal source that is defined in (12), where M is the signal generation function of the multipath element, P is the amplitude modulation factor that is typically less than one, ϕ is a randomly generated - static phase-shift between 0 and 2π, and τ represents the delay of the input timing vector that accounts for the extra distance that the reflected signal had to travel with respect to the direct signal. If $[T]$ is an $[L \times 1]$ vector then $[M]$ will also be a $[L \times 1]$ vector.

$$[M] = PAe^{i2\pi f_c([T]-\tau)}e^{i\phi} \tag{13}$$

3.1.3 *Signal Generation and Reception*

This section will detail how the M&S environment simulates sample-level data with computational efficiency. Figure 5 shows a simple case where two sources and one receive antenna are present in the environment; the discussion in this section steps through the simulation process for this example.

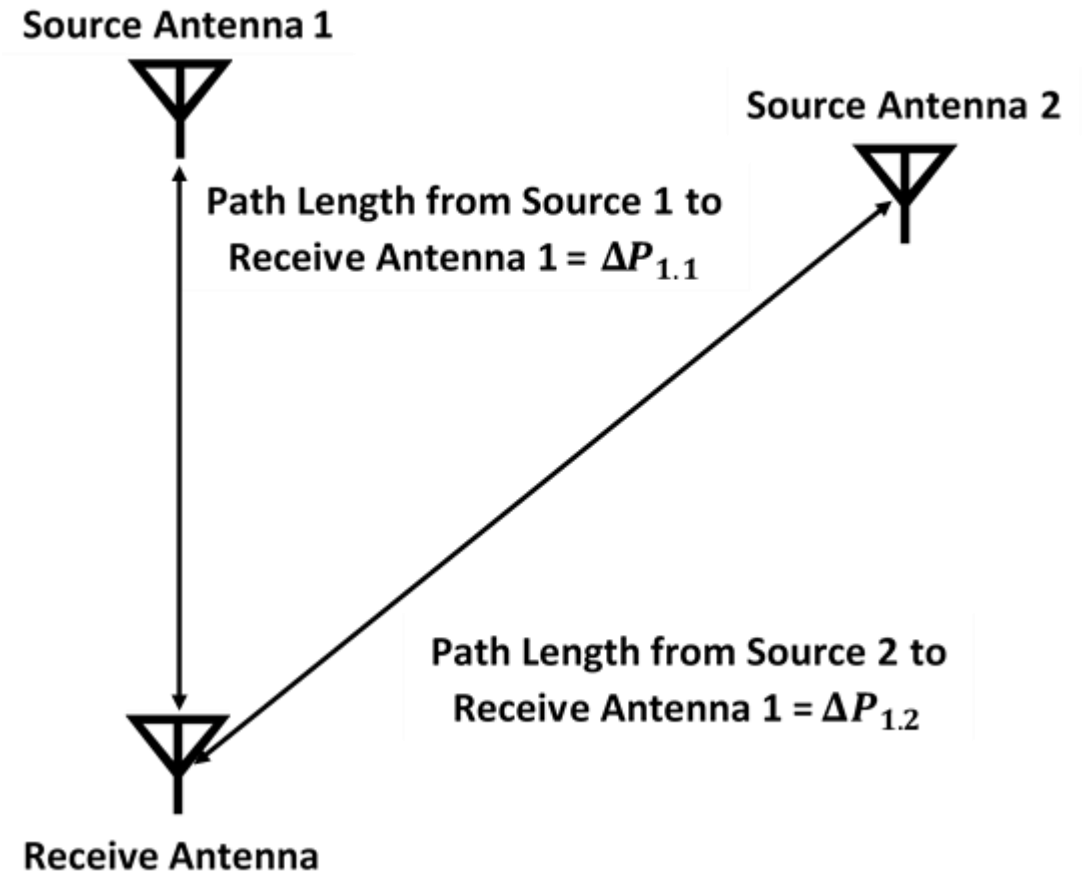

Figure 5. Signal Generation and Reception Example Scenario

To achieve computationally efficient simulation of RF signals, the simulator begins by generating a time sampling vector, $[T]$, for each source and each receive antenna. These times begin at zero and increase according to a sampling rate, $t_{sample} = \frac{1}{f_{sample}}$, that is defined at the outset of the simulation according to the sampling rate of the analog to

digital converter (ADC). The general time sampling vector, $[T]$, for L samples is shown in (14).

$$[T] = \left[0, t_{sample}, 2t_{sample}, \dots, (L-1)t_{sample}\right]^T \tag{14}$$

Next, the distances between each transmission source and each receiver location are calculated, divided by the speed of light, and subtracted from the timing vector; this process yields a vector of times for each transmission source for every receive element. For M transmission sources and N receive antennas $M \times N$ timing vectors are generated; these vectors have the naming convention: $\left[T_{receiver,source}\right]$. Equations (15-16) show the timing vectors for each transmission source in the example of Figure 5 where c is the speed of light.

$$\left[T_{1,1}\right] = [T] - \Delta P_{1,1}/c \tag{15}$$

$$\left[T_{1,2}\right] = [T] - \Delta P_{1,2}/c \tag{16}$$

Once the timing vectors are calculated, the vectors that correspond to a given source are found according to the signal generation function that was defined for that source in the antenna definition. It must be a complex function that is continuous for all time. Let S_1 and S_2 be the complex signal generation functions that have been defined for sources one and two, respectively. Also define the complex sample vectors that are generated by each source and are received by the receive antenna as $[\boldsymbol{S_{1,1}}]$ and $[\boldsymbol{S_{1,2}}]$ according to the convention: $[\boldsymbol{S_{receiver,\ source}}] = S_{source}[T_{receiver,\ source}]$; then the sample vectors for the receiver are calculated as shown in (17-18).

$$[\boldsymbol{S_{1,1}}] = S_1[T_{1,1}] \tag{17}$$

$$[\boldsymbol{S_{1,2}}] = S_2[T_{1,2}] \tag{18}$$

Finally, the sample vector received at the antenna is the sum of these two vectors according to the convention $[\boldsymbol{S_{receiver}}]$. Therefore, the RF in-phase and quadrature sample data at the receive antenna is given by (19).

$$[\boldsymbol{S_1}] = [\boldsymbol{S_{1,1}}] + [\boldsymbol{S_{1,2}}] \tag{19}$$

This process is repeated for each receive antenna in the environment, Figure 6 shows the flow chart that is generalized to show the calculation of the RF sample data for *M* transmission sources and *N* receive antennas.

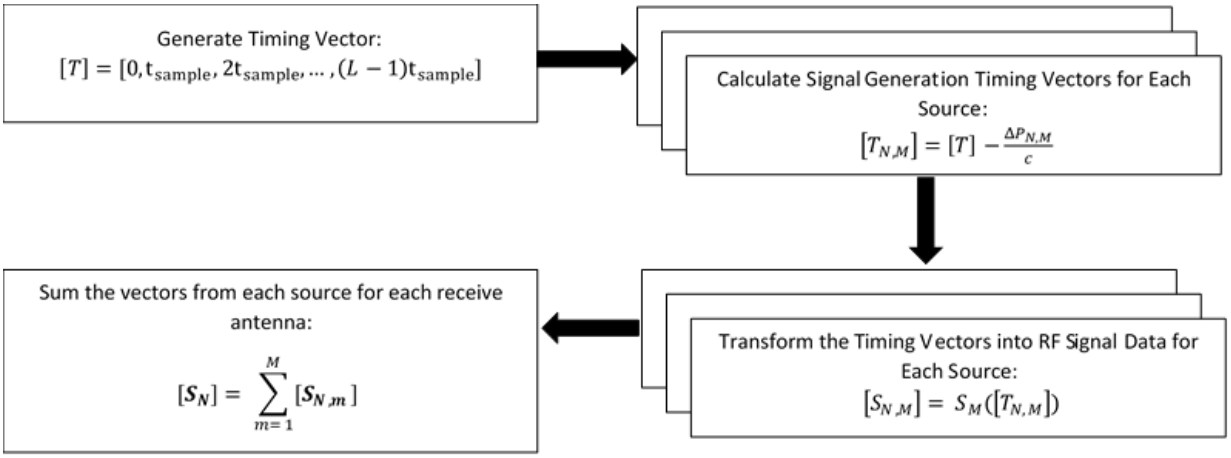

Figure 6. Signal Generation Algorithm for M Sources and N Receive Antennas

These RF samples can be manipulated for any desired application. For this effort the samples are downconverted to an intermediate frequency (IF) of 10 MHz and then low-pass filtered before being sampled.

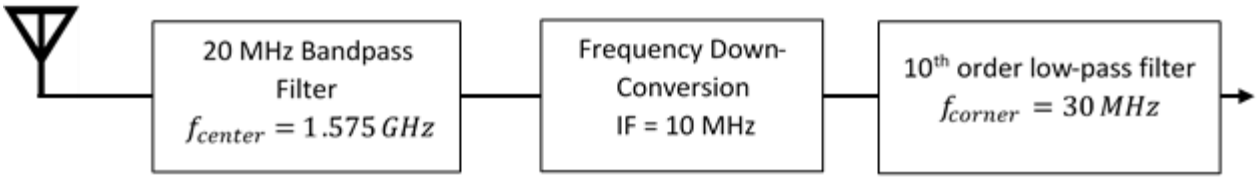

Figure 7. Receive Chain for a Single Antenna Element

When multiple receiver locations are grouped into a receive array these vectors can be stored as an $[N \times L]$ sampling matrix where N is the number of receive elements and L is the number of samples. For this research the sampling matrix, (20), is $[6\ x\ 1024]$, and is assumed to be zero-mean.

$$X_{sample} = \begin{bmatrix} x_{1,1} & \cdots & x_{1,L} \\ \vdots & \ddots & \vdots \\ x_{N,1} & \cdots & x_{N,L} \end{bmatrix} \tag{20}$$

The sampling matrix can be modified to model thermal noise if desired, see (39) for the noise model in this effort. After the sampling matrix is obtained, the sampling covariance matrix, C, is estimated as follows:

$$C = X_{sample} X_{sample}^{H} \tag{21}$$

The covariance matrix is a complex, symmetric $[N \times N]$ matrix constructed of all of the samples in the sampling matrix. It has been shown that more samples can improve AoA performance and that the lower bound on the standard deviation of AoA errors from any unbiased AoA algorithm is inversely related to the square root of the number of samples used [17] [18].

3.2 Angle-of-Arrival Estimation Algorithms

In this section four passive AoA algorithms are presented, and it is explained how each algorithm estimates the AoA of interference sources.

3.2.1 *Phase-shift Beam Forming*

The Phase-shift Beamformer (PSBF) is the most straight-forward method. It is described in (22), where $P_{PSBF}(\theta)$ is the power output from the algorithm as a function of AoA, $A(\theta)$ is the array manifold as a function of theta as calculated in (7), and C is the estimated covariance matrix from (21).

$$P_{PSBF}(\theta) = abs(A(\theta)^{\mathrm{H}}\, C\, A(\theta)) \tag{22}$$

For any given AoA, the samples of each element are phase-shifted to account for the difference in the time-of-arrival (ToA) for a plane-wave from that direction and are summed. If the phase-shifts are the inverse of the ToA-induced phase differences at the antenna elements, then the sum of the samples will be coherent. Therefore, each AoA in the field of regard (FOR) has a unique set of phase weights that can be treated as an AoA hypothesis. The PSBF applies each set of phase-shifts to the sampling covariance matrix to test each hypothesis. When a hypothesis closely matches the AoA of an interference source measurable peaks are produced, as shown in Figure 8.

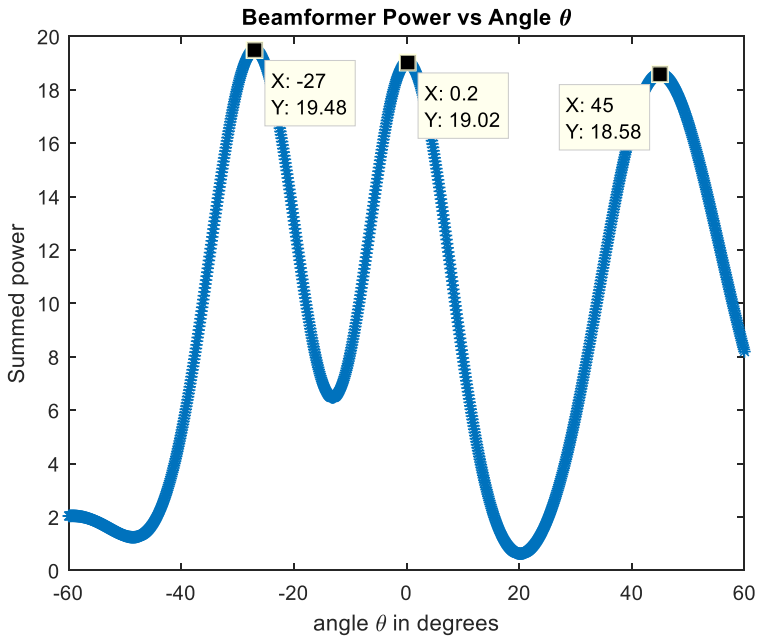

Figure 8. PSBF Output for Sources at -26.6, 0.0, and 45.0 Degrees

PSBF is the simplest method analyzed in this effort and has the lowest computational burden of any of the methods studied. Each angle hypothesis requires only two matrix multiplications to generate the output. In practice all angles in the FOR can be calculated in parallel which can further reduce computing time.

3.2.2 *Capon's Beamformer*

Capon's beamformer was originally proposed by J. Capon for applications in seismology, and is often called the Minimum Variance Distortionless Response (MVDR) beamformer [9]. Capon beamforming is described in (23), where $P_{Capon(\theta)}$ is the output of the beamformer as a function of the AoA hypothesis, $A(\theta)$ is the array manifold from (7), and C^{-1} is the inverse of the estimated covariance matrix.

$$P_{Capon}(\theta) = abs\left(A(\theta)^{\mathrm{H}} C^{-1} A(\theta)\right)^{-1} \quad (23)$$

This method is derived by considering the angle hypothesis that will minimize the amount of energy entering into the receiver. To use Capon's beamformer note that the covariance matrix must be invertible. This is generally the case so long as the covariance matrix estimate is based on a number of samples that is much larger than the size of the matrix. For the purposes of this study we can always assume the covariance matrix is invertible since $1024\ samples \gg 6\ elements$. A derivation of the Capon beamformer is given below.

For any given environment there exists an angle hypothesis that will minimize the energy received. Let *b* be a length *N* vector that represents the energy in the receiver from each receive element subject to phase-shifting from the angle hypothesis $A(\theta)$ that was derived in (7) that is also a length *N* vector. Then the antenna can be represented as the linear system:

$$C^{-1}A(\theta) = b \quad (24)$$

Then the least-squares minimization of the system is an angle hypothesis $A(\theta)$ that is a solution to:

$$C^H C A(\theta) = C^H b \quad (25)$$

Since the covariance matrix, and therefore its Hermitian, is invertible this quickly reduces to:

$$A(\theta) = C^{-1}b \tag{26}$$

To apply this result to the AoA problem, recall that entries of *b* are the samples at the individual antenna elements in the array. Therefore, when a plane wave is incident on the array for some θ, and a real constant *d*:

$$b = d\overline{A(\theta)} \tag{27}$$

For the AoA problem we can safely assume that the constant *d* is inconsequential to the result and can be set to unity, thus:

$$b = \overline{A(\theta)} \tag{28}$$

Next, consider the PSBF that is composed of these weights:

$$P(\theta) = abs\left(\left(C^{-1}\overline{A(\theta)}\right)^H C\, C^{-1}\overline{A(\theta)}\right) \tag{29}$$

$$= abs\left(\overline{A(\theta)}^H (C^{-1})^H \overline{A(\theta)}\right) \tag{30}$$

$$= abs\left(\left(\overline{A(\theta)}^H (C^{-1})^H \overline{A(\theta)}\right)^H\right) \tag{31}$$

$$= abs\left(\overline{A(\theta)}^H C^{-1} \overline{A(\theta)}\right) \tag{32}$$

$$= abs(A(\theta)^H C^{-1} A(\theta)) \tag{33}$$

To be consistent with the convention that a measurement peak indicates a signal source, a constant is divided by the output of the beamformer, (34), yielding the Capon beamformer.

$$P_{Capon}(\theta) = \frac{1}{abs\left(A(\theta)^{\mathrm{H}} C^{-1} A(\theta)\right)} \tag{34}$$

In more direct terms, Capon's method works by projecting a hypothesis onto the inverse of the covariance matrix; this steers a destructive interference or "null" at the hypothesized location. When the null coincides with the direction of an energy source the power received dramatically decreases. To put this into common terms with PSBF and maintain the convention of a local maxima indicating the presence of an energy source, the inverse of the estimate is presented as a pseudo power. An example of the output of the Capon algorithm is shown in Figure 9.

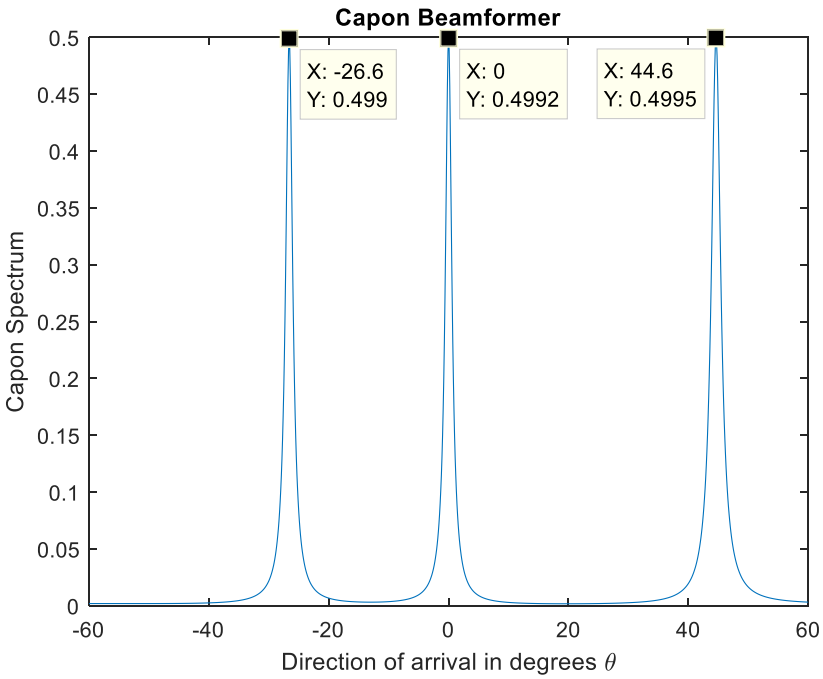

Figure 9. Capon Output for Sources at -26.565, 0.0, and 45.0 Degrees

The local maxima of this function are compared to a threshold and if they are large enough compared to the noise floor, they are considered legitimate detections. The Capon method yields much sharper peaks than the PSBF indicating improved potential for fine resolution of closely spaced sources. In practice, the angle hypotheses can be computed in parallel for increased computing speed. The drawback of the Capon beamformer relative to the PSBF is the inverse of the estimated covariance matrix must be computed.

3.2.3 *Multiple Signal Identification and Classification*

Multiple Signal Identification and Classification (MUSIC) was introduced as an array signal processing technique for finding AoA by R.O. Schmidt [10]. The MUSIC algorithm expands on the null-steering theme of the Capon beamformer by applying a singular value decomposition of the covariance matrix to separate it into an orthonormal basis of

eigenvectors and their associated eigenvalues. This process is described in (35) where the matrix *U* is a unitary matrix representing the orthonormal basis of eigenvectors and $\sum$ is a diagonal matrix containing the eigenvalues of the covariance matrix.

$$SVD(C) = U\sum V^H = U\sum U^H \tag{35}$$

The matrix *U* can be partitioned to separate the signal subspace from the noise subspace. This partition is accomplished by examining the size of the eigenvalues and thresholding them against the established level of the noise floor. By establishing a threshold for the eigenvalues, the *U* matrix can be separated into a space that corresponds to the interference sources and a space that corresponds to background noise. The number of columns of U_{signal} also serves as an estimation of the number of signal sources present.

$$U = [U_{signal}, U_{noise}] \tag{36}$$

Finally, the MUSIC spectrum is formed by projecting each AoA hypothesis onto the noise subspace. When the beam approaches the area where the signal sources reside, the power received by the projection drops dramatically; in a noiseless environment it will approach zero. As with the Capon method the output of the MUSIC algorithm, given in (37), is inverted to create a sharp peak to indicate the presence of a signal source at a given angle θ.

$$P_{MUSIC}(\theta) = abs(\frac{1}{A(\theta)^H U_{noise} U_{noise}^H A(\theta)}) \tag{37}$$

An example of the output of the MUSIC algorithm is shown in Figure 10.

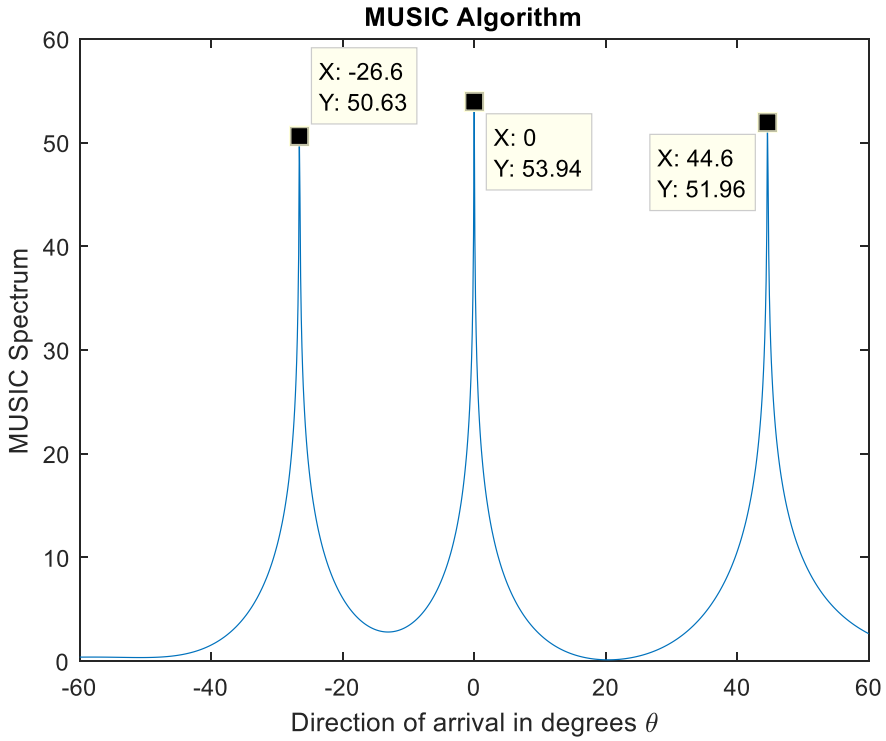

Figure 10. MUSIC Algorithm with Sources at -26.65, 0.0, and 45 Degrees

Relative to the Capon method, the MUSIC algorithm has a greater peak-to-null ratio and similarly sharp peaks which indicate capability for fine resolution of closely spaced sources. MUSIC as presented in this thesis involves some increased computational complexity over the Capon beamformer, it requires some increased logic to separate the signal and noise subspaces, and it requires one additional matrix multiplication. In practice the angle hypotheses can be computed in parallel, which may increase computing speed.

3.2.4 *Maximum Likelihood Estimation*

The Maximum Likelihood Estimation (MLE) algorithm is a straightforward concept. Any *N*-element array is capable of steering *N-1* beams or nulls simultaneously [29]. MLE as

implemented in this study simultaneously steers *N-1* beams to maximize the power received. This technique attempts to solve an *N-1* dimensional optimization problem; it is an iterative process that will search the *N-1* dimensional beamspace to maximize power. This research uses the alternating projection algorithm proposed by I. Ziskind and M. Wax as a computationally efficient way to handle the multidimensional optimization problem [30]. This method varies the solution in one dimension at a time finding the local maximum in that dimension. Each dimension is varied in this way until the local maxima for the solution is reached. Because of the iterative "hill climbing" nature of the algorithm, it may not find the global maximum and may instead settle on a local maximum. Therefore, intelligent initialization of the MLE algorithm is vital to finding the correct solution. For this effort, the algorithm was initialized by taking *N-1* largest values produced by the output of the PSBF algorithm. Additionally, the practical resolution of the beams being used must be considered to avoid multiple beams settling on the strongest source and the algorithm becoming blind to weaker signal sources in the environment. A flow-chart description of the MLE alternating projection algorithm is shown in Figure 11.

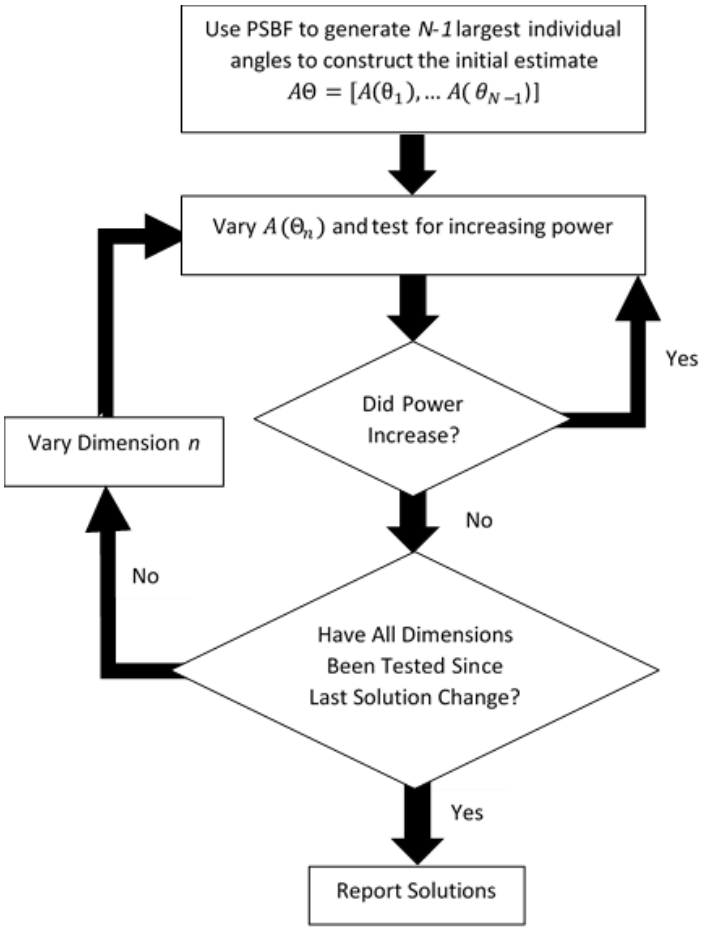

Figure 11. MLE Alternating-Projection Algorithm Flowchart

Where the matrix $A\Theta$, given in (38), is a $[N \times (N-1)]$ matrix with columns that represent the array manifold for a single beam directed at an angle θ as defined in (7).

$$A\Theta = [A(\theta_1), \ldots, A(\theta_{N-1})] \tag{38}$$

As an iterative algorithm, MLE is much more computationally complex than any of the others presented. Iteration continues until the solution converges below some established threshold. In practice, the number of iterations must be limited according to the constraints

of the implementation. For all the results in this research, the number of iterations is arbitrarily limited to ten.

The output of the MLE algorithm is a list of angles that are most likely to have interference sources. As implemented, it does not deliver an estimate of the number of sources present in the environment but instead always searches for *N-1* individual power sources.

3.3 Algorithm Complexity Analysis

While performance is the focus of this study it is valuable to assess the complexity of the solutions as context for comparing their performance. For comparison purposes the co-variance matrix, which is computed in firmware in real-time, is neglected because it must be accomplished for all algorithms; for the same reason the function for finding the local maxima of the output of the AoA algorithm is also neglected. What is compared is the number of operations required to compute the output of the algorithm for a given angle. Also compared are setup operations; these being operations that must be accomplished before the solutions can be computed for each angle. Table 1 summarizes the complexity comparisons for the four algorithms based on implementation for a six element ULA. Operations are reported as complex floating-point operations. This analysis is only a direct comparison of complexity and does not consider possible optimization. For example, matrix inversion is counted as N^3 operations when it may be less depending on the implementation and the size of the matrix. The MUSIC algorithm will vary slightly depending on the size of the noise subspace; this comparison shows a worst-case example where the noise subspace is large.

Table 1. Algorithm Complexity Comparison

Algorithm	Setup Operations	Setup Operations per Solution	Operations per θ Hypothesis	# Operations per θ Hypothesis
PSBF	N/A	N/A	2 Matrix Multiplications	42
Capon	1 Matrix Inversion	216	2 Matrix Multiplications, 1 Division	43
MUSIC	1 SVD, 1 Matrix Multiplication, 1 Thresholding	402	2 Matrix Multiplications, 1 Division	43
MLE	N/A	N/A	N/A	630 – 6300*

To use this table consider using the MUSIC algorithm with a 1° resolution over a ±60° FOR. The number of setup operations is 402 and the number of operations for all hypothesis is $121 \times 43 = 5{,}203$, thus the total number of operations is 5,245. At finer resolutions, the number of setup operations becomes small compared to the total number of operations. For example, using MUSIC with .1° resolution over a ±60° FOR requires 51,643 operations to calculate every hypothesis and 402 setup operation for a total of 52,045 operations.

Computationally, PSBF is the simplest algorithm requiring only two matrix multiplications. The Capon beamformer adds a single division for each angle and requires a matrix inversion prior to computation. The MUSIC algorithm requires the singular value decomposition, a matrix multiplication as well as thresholding prior to determining the

angles; it also requires an additional matrix multiplication and division for each angle, compared with the PSBF. MLE is by far the most complex. Due to the iterative nature of the algorithm, the complexity of MLE is unpredictable but will generally vary from one to two orders of magnitude above the other methods. This is due to the large amount of "guess and check" computing that is required to solve the optimization problem. None of the closed-form algorithms (i.e. PSBF, Capon and MUSIC) are complex enough to significantly influence algorithm choice. However, MLE may be too cumbersome depending on the resources available at implementation.

IV. Results

This section details the test results for the Phase-shift Beamformer (PSBF), the Capon beamformer, the Multiple Signal Identification and Classification (MUSIC) algorithm, and the Maximum Likelihood Estimation (MLE) algorithm. Each section describes the test, shows the results, and briefly comments on the results. All results in this thesis are simulated by modeling the antenna and hardware described in Section II with the modeling and simulation (M&S) environment described in Section III. Studies that include significant random factors, such as the signal to noise ratio (SNR) test and the multipath test are displayed as Monte` Carlo simulations. Results that had no significant random elements are displayed in tables. Each test is designed to exclude other sources of error when possible. For example, the SNR Monte` Carlo in Section 4.2 will show SNR induced errors are very close to zero when the SNR is greater than 10 dB; every subsequent test set SNR to at least 20 dB in order to examine the effects of other error inducing phenomena.

4.1 Chamber Data Test

This test ensures that the simulation environment and the algorithms function properly. Data captured by the antenna array in an anechoic chamber is introduced to the model, and replaces the simulated sample data. The data used is the in-phase and quadrature sampled output of the array after it has been calibrated by the manufacturer. The goal of this test is to show that the M&S environment created for this research is a realistic, usable tool that is compatible with the hardware that the angle-of-arrival (AoA) algorithms will support.

4.1.1 *Chamber Data Test Results*

The chamber data test results show three separate AoA measurements in an anechoic chamber. The true AoAs of the sources in the chamber are -45°, 0°, and 45°. The results are shown in Table 2.

Table 2. Chamber Test Data Results

AoA Truth	-45.0°	0.0°	45.0°
PSBF	-44.9°	0.0°	42.9°
Capon	-47.1°	0.0°	40.8°
MUSIC	-48.3°	0.0°	42.5°
MLE	-52.3°	0.0°	42.8°

The chamber test verifies the simulation environment and shows the algorithms created are capable of measuring AoA using data collected from the physical antenna. It also underscores the importance of measuring, rather than calculating, the array manifold; ideally all of the measurements would be perfect considering this data was collected in a pristine environment. However, because of non-ideal conditions within the array, the true array manifold does not perfectly match the one calculated in Section II; creating significant AoA measurement errors.

4.2 Signal to Noise Ratio Monte' Carlo

Every algorithm will require some minimum SNR to function correctly. To establish the SNR required a Monte` Carlo simulation is accomplished. To be consistent with the hardware definition presented in Section II the number of antenna elements is $N = 6$ and the number of samples, L, was held constant at 1024, which represents 15.75 μs of sampled data, all sensitivities found here could be improved with more samples and a longer integration time. Each algorithm solved the AoA of three sources in the FOR. Each source had an SNR value that varied from -20 to +10, with one hundred runs accomplished at every SNR. The outputs of this study are the error mean, error standard deviation and the algorithm failure rate. Algorithm failure occurs when an algorithm reports too many or too few sources in the environment, in this case the run is not used to calculate error statistics. For this research an algorithm is considered robust at a given SNR so long as its algorithm failure rate remains below fifty percent and its mean error is below one degree. Equation (39) shows the signal model used for this simulation where X_{sample} is the $[N \times L]$ block of samples used to estimate the AoA and each ϵ is a zero-mean gaussian random variable.

$$X_{sample+error} = X_{sample} + 10^{-\frac{SNR}{20}}\left(\begin{bmatrix} \epsilon_{1,1} & \cdots & \epsilon_{1,L} \\ \vdots & \ddots & \vdots \\ \epsilon_{N,1} & \cdots & \epsilon_{N,L} \end{bmatrix} + i\begin{bmatrix} \epsilon_{1,1} & \cdots & \epsilon_{1,L} \\ \vdots & \ddots & \vdots \\ \epsilon_{N,1} & \cdots & \epsilon_{N,L} \end{bmatrix}\right) \quad (39)$$

The standard deviation of the random variables, as it relates to the power of the noise signal, is treated as the independent variable and the AoA solutions from each algorithm

are treated as dependent variables. Three sources are present in the environment and are located at 45, 0, and -30 degrees.

4.2.1 *Signal to Noise Ratio Monte' Carlo Results*

The results for the PSBF are shown in Figure 12.

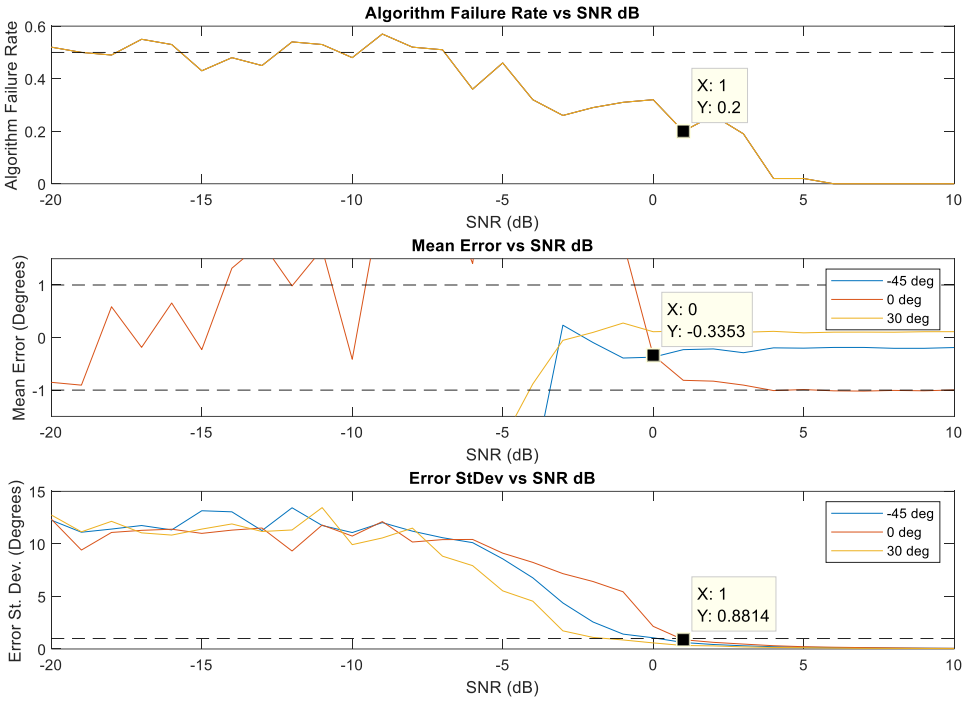

Figure 12. PSBF SNR Monte' Carlo Results

The failure mode for the PSBF was mean error greater than one degree. Failure occurred at SNRs below 0 dB; the algorithm failure rate was 32% at this level. AoA error standard deviation exceeded one degree at SNRs lower than 1 dB; algorithm failure rate was 20% at this level. The PSBF algorithm performance became usable around 0 dB and excellent above 5 dB. The results for the Capon beamformer are shown in Figure 13.

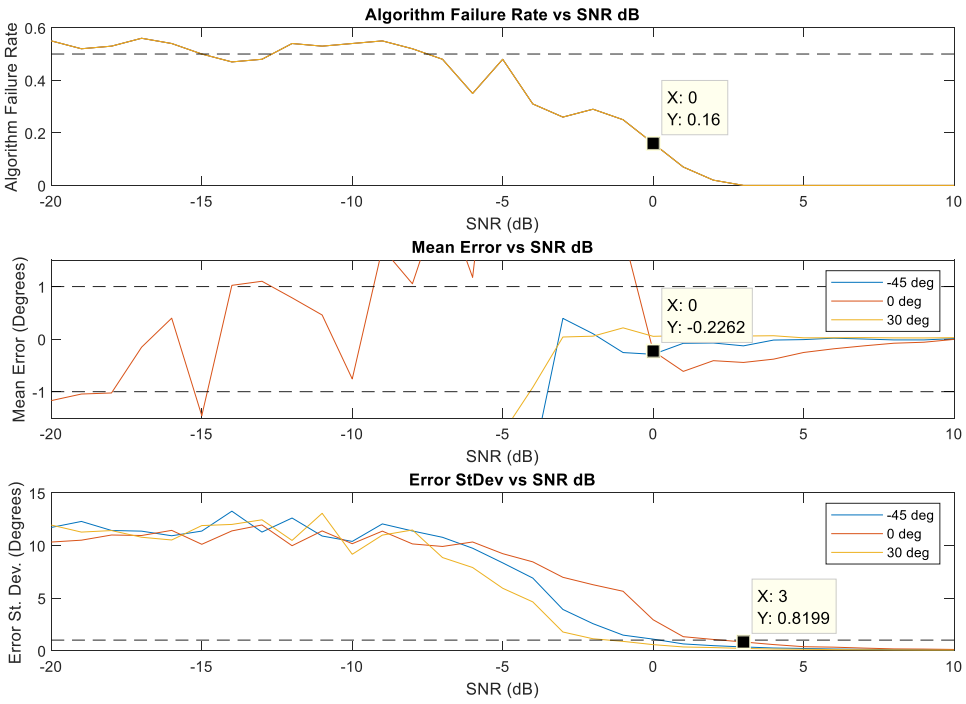

Figure 13. Capon SNR Monte' Carlo Results

The failure mode for the Capon was mean error greater than one degree. Failure occurred at SNRs below 0 dB; the algorithm failure rate was 16% at this level. AoA error standard deviation exceeded one degree at SNRs lower than 3 dB; algorithm failure rate was 0% at this level. The Capon beamformer performance became usable around 0 dB and excellent above 3 dB. The results for the MUSIC algorithm are shown in Figure 14.

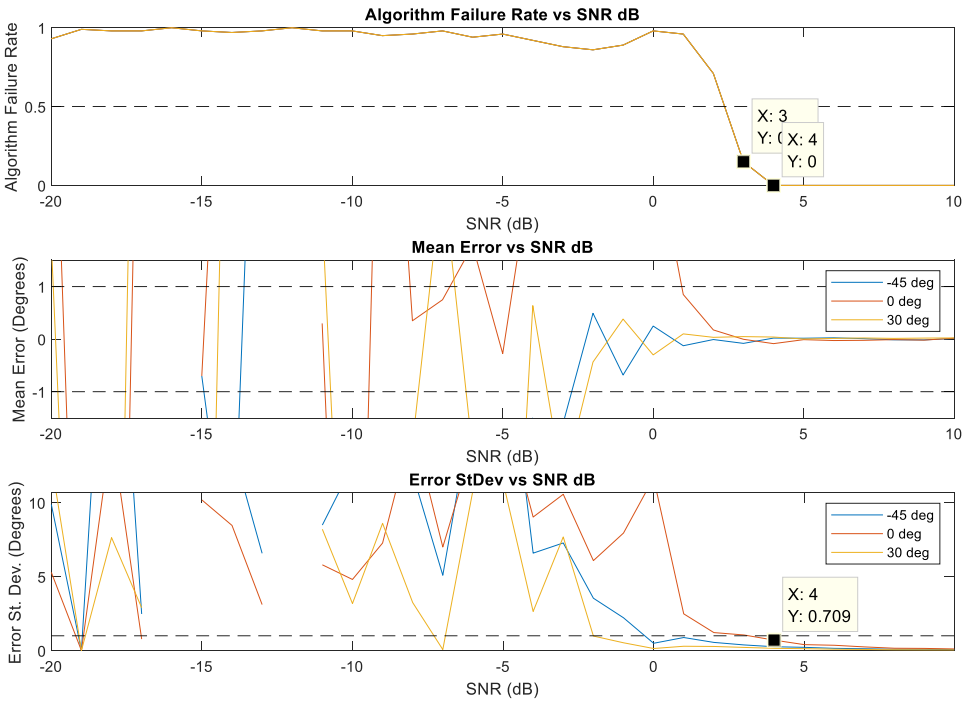

Figure 14. MUSIC SNR Monte' Carlo Results

The failure mode for the MUSIC was algorithm failure rate greater than fifty percent. Failure occurred at SNRs below 3 dB; mean error was negligible at this level. AoA error standard deviation exceeded one degree at SNRs lower than 4 dB; algorithm failure rate was 0% at this level. The MUSIC algorithm performance became usable at 3 dB and excellent above 3 dB. The results for the MLE algorithm are shown in Figure 15.

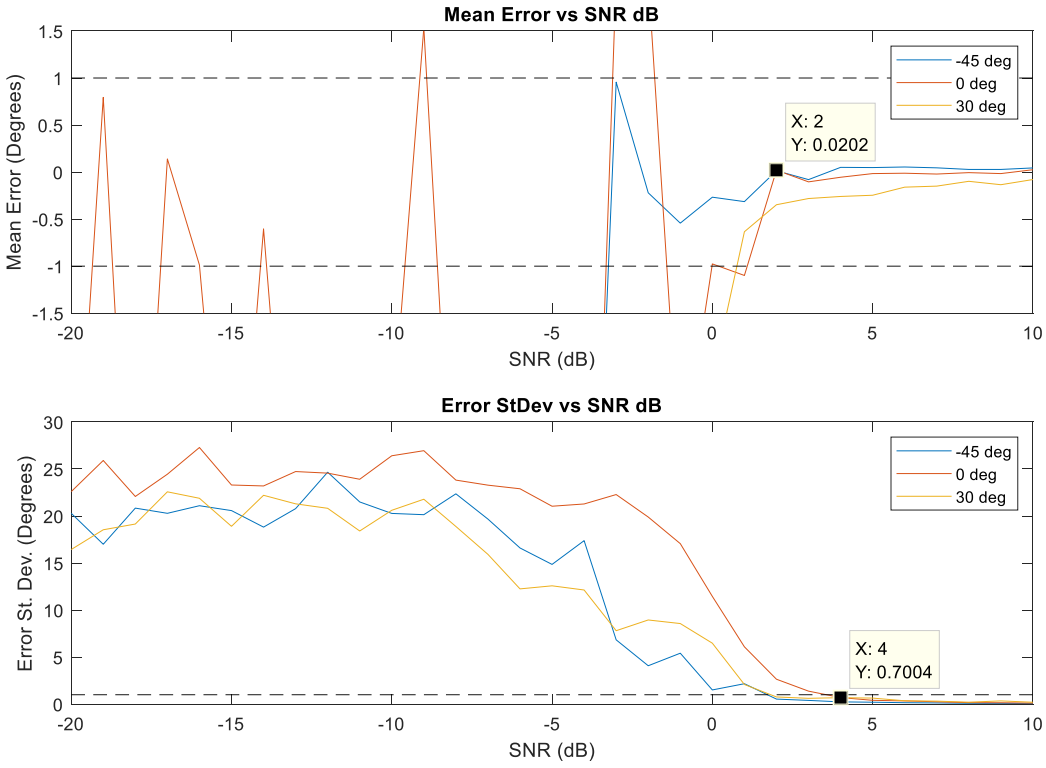

Figure 15. MLE SNR Monte' Carlo Results

Since MLE does not report the number of sources in the environment it does not have an algorithm failure rate. Instead it may point a beam in an erroneous location and report a detection. This causes the mean and standard deviation error statistics to appear as though they degrade faster than the other algorithms when that may not be the case when considering the algorithm failure rate of the other methods. Therefore, accurate comparisons of one of the other algorithms with the MLE is most valuable when the algorithm failure rate is near to zero. Failure occurred at error SNRs lower than 2 dB. AoA error standard deviation exceeded one degree at SNRs lower than 4 dB. In general, MLE was usable with SNR levels greater than 2 db. It is worthwhile to mention that the PSBF has relatively graceful degradation until SNR near 0 dB.

4.2.2 *Signal to Noise Ratio Monte` Carlo Test Summary*

In general, the methods that use constructive interference patters, PSBF and MLE, were more sensitive due to the antenna gain realized by the constructive patters. The destructive interference techniques, Capon and MUSIC, were less sensitive. In general SNR levels of 6 dB or greater were sufficient for AoA estimation. These results are consistent with previous works comparing PSBF, MUSIC and Capon [27] with the exception of the Capon algorithm. In this simulation it outperforms MUSIC in the low-SNR region while in the previous work it performed much worse. The previous works did not detail the noise model used, and so conclusions are difficult to draw. One possible explanation is that thesis models thermal noise present in the receiver rather than environmental noise. Environmental noise is attenuated by antenna gain, and subspace decomposition while thermal noise is omnipresent. This may also explain differences in MUSIC performance vs SNR curves described in other published works [16].

4.3 Complex Environment Test

It has been shown that there is a limit to the number signal sources that can be unambiguously resolved from an *N*-element antenna array is limited to *N-1* [29]. This limitation applies to all of the algorithms analyzed in this effort. To test the failure states when the environment becomes too complex, each algorithm is run with an increasing number of sources in the field of regard (FOR). Each source is inserted into the environment with 40 dB signal to noise ratio (SNR) and with adequate spatial separation for each algorithm to resolve each individual source.

4.3.1 *Two source Test*

For the first test, two sources are placed within the FOR and are placed at -30 and 30 degrees. The results are included in Table 3.

Table 3. AoA Solutions with Two Sources in the Environment

AoA Truth	-30.0°	30.0°
PSBF	-26.8°	26.8°
Capon	-30.0°	30.0°
MUSIC	-30.0°	30.0°
MLE	-30.0°	-29.9°

All algorithms were able to detect both sources, the PSBF had the most error; its power as a function of angle is shown in Figure 16.

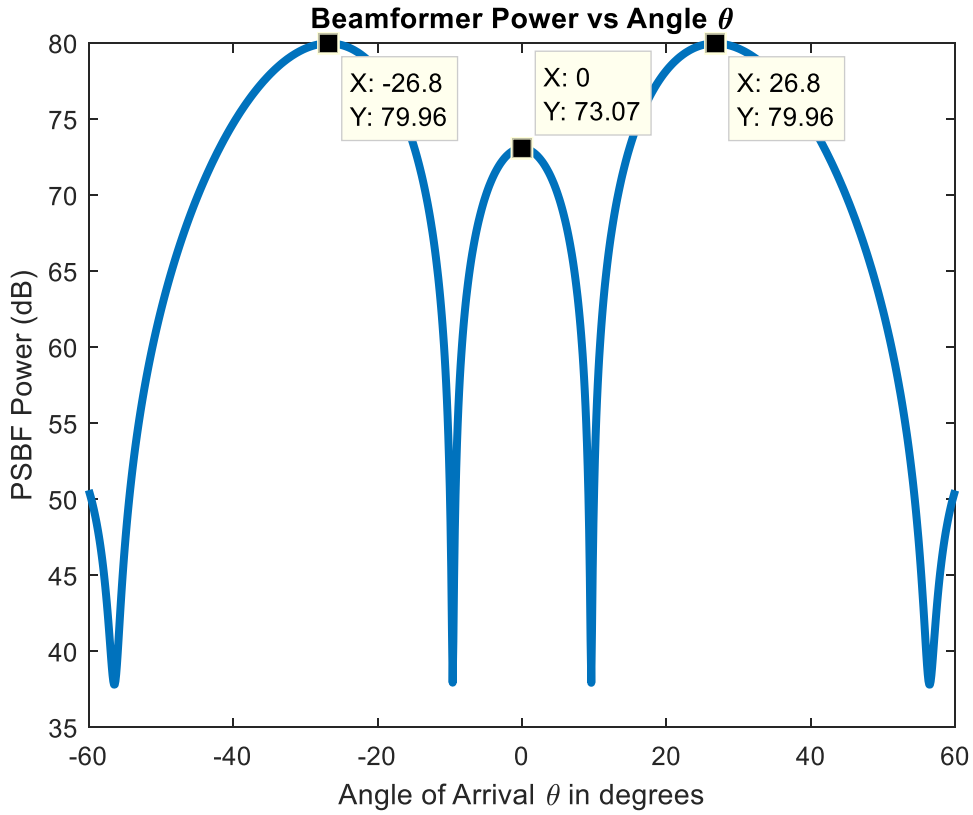

Figure 16. PSBF Output for the Complex Environment Test with Two Sources

Figure 12 shows that the solutions for the PSBF are drawn towards one another due to energy from the off-angle source entering through the sidelobes of the beam. This phenomenon is a known issue with the PSBF. An unexpected issue in this test is the false alarm at zero degrees. The two sources each created a sidelobe and the two sidelobes constructively added at zero degrees to create a peak that registered as a false detection since it is only 6.89 dB below the actual peaks. In contrast, Figure 17 shows the output of the MUSIC algorithm for the same test.

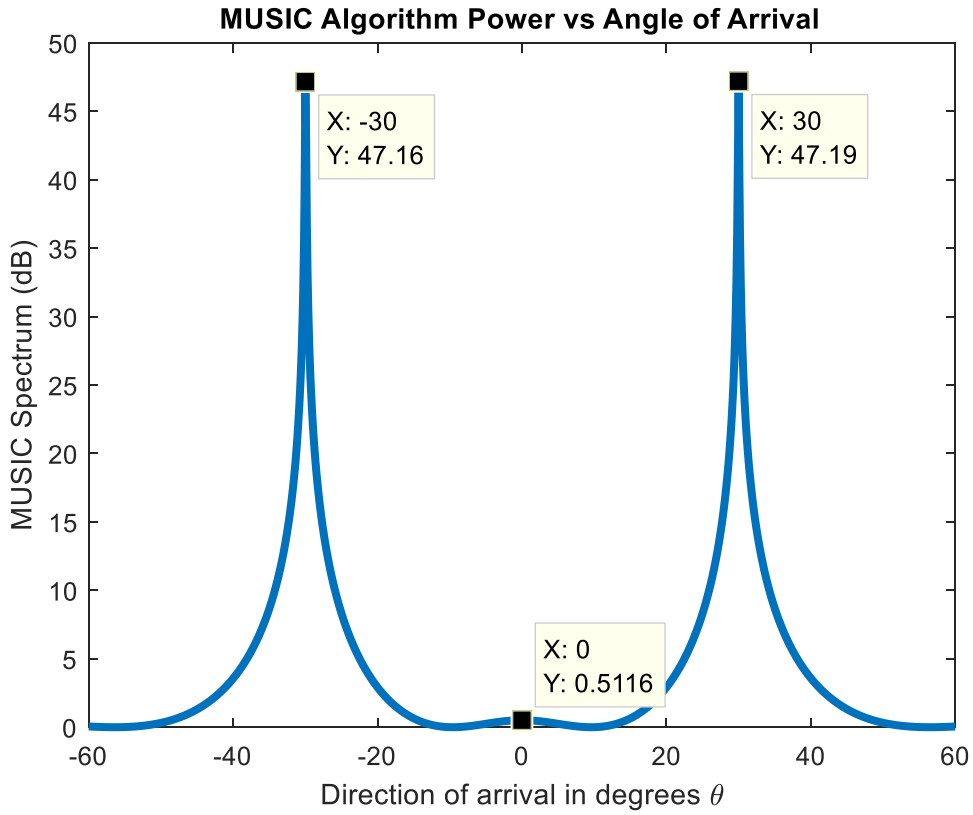

Figure 17. MUSIC Output for the Complex Environment Test with Two Sources

The output for the MUSIC algorithm shows that the two peaks are unaffected by the energy from the other. At zero degrees there is some noticeable increase in output power, but it is -46.6 dB from the peaks and well below the detection threshold for the algorithm.

4.3.2 *Three Source Test*

For this test, three sources are placed within the FOR and are placed at -45, 0 and 45 degrees. The results are included in Table 4.

Table 4. AoA Solutions with Four Sources in the Environment

AoA Truth	-45.0°	0.0°	45.0°
PSBF	-46.0°	0.4°	46.0°
Capon	-45.0°	0.0°	45.0°
MUSIC	-45.0°	0.0°	45.0°
MLE	-45.6°	0.2°	45.9°

4.3.3 *Four Source Test*

For this test, four sources are placed within the FOR and are placed at -45, -15, 15 and 45 degrees. The results are included in Table 5.

Table 5. AoA Solutions with Four Sources in the Environment

AoA Truth	-45.0°	-15.0°	15.0°	45.0°
PSBF	-45.8°	-14.4°	14.3°	45.8°
Capon	-45.0°	-15.0°	15.0°	45.0°
MUSIC	-45.0°	-15.0°	15.0°	45.0°
MLE	-44.78°	-14.35°	15.05°	46.1°

4.3.4 *Five Source Test*

For this test, five sources are placed within the FOR and are placed at -58, -30, 0, 30 and 58 degrees. The results are included in Table 6.

Table 6. AoA Solutions with Five Sources in the Environment

AoA Truth	-58.0°	-30.0°	0.0°	30.0°	58.0°
PSBF	N/A	-29.6°	°0.0	29.6°	N/A°
Capon	-58.0°	-30.0°	°0.0	30.1°	57.9°
MUSIC	-58.0°	-30.1°	°0.0	30.1°	57.9°
MLE	-56.4°	-30.2°	°0.0	31.6°	60.0°

Here the PSBF failed to find the sources at +/-58° this is due to the peaks becoming obscured at the edges of the field of view. Figure 14 shows the output of the PSBF algorithm.

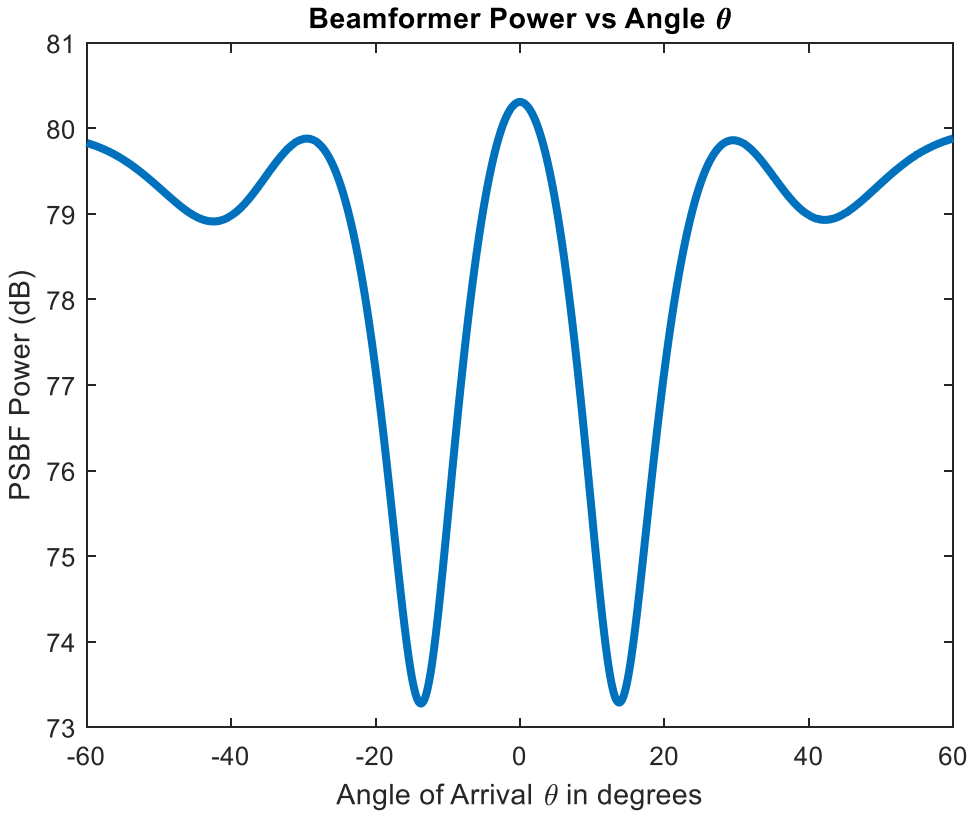

Figure 18. PSBF Output for the Complex Environment Test with Five Sources

The energy in the PSBF in Figure 18 at +/-58° does not fall at +/-59° or +/-60°; this is most likely due to sidelobe energy from the other sources bleeding into the solution. As a result, the algorithm is unable to determine the presence of a peak despite the local increase in energy.

It is noteworthy that the MLE algorithm accurately detected these sources because it seeks to maximize energy when simultaneously steering five beams and therefore it does not rely on peak detection in the same way as the other algorithms.

4.3.5 *Six Source Test*

For this test, six sources are placed within the FOR and are placed at -50, -30, -10, 10, 30 and 50 degrees. Each source has a SNR of 40 dB. The results are included in Table 7.

Table 7. AoA Solutions with Six Sources in the Environment

AoA Truth	-50.0°	-30.0°	-10.0°	10.0°	30.0°	50.0°
PSBF	-41.9°	N/A	-13.6°	°13.2	N/A	41.6°
Capon	-41.8°	N/A	-14.9°	°14.7	N/A	41.6°
MUSIC	-41.6°	-18.4	-1.1°	°18.0	N/A	41.6°
MLE	-41.5°	-16.4°	-1.1	°18.0	N/A	41.6°

Errors for all four algorithms grow massively for the six-source case. Analysis of the output of each algorithm makes it unclear as to whether the outputs have any meaning. Figures 19-21 show the output of the PSBF, Capon, and MUSIC techniques.

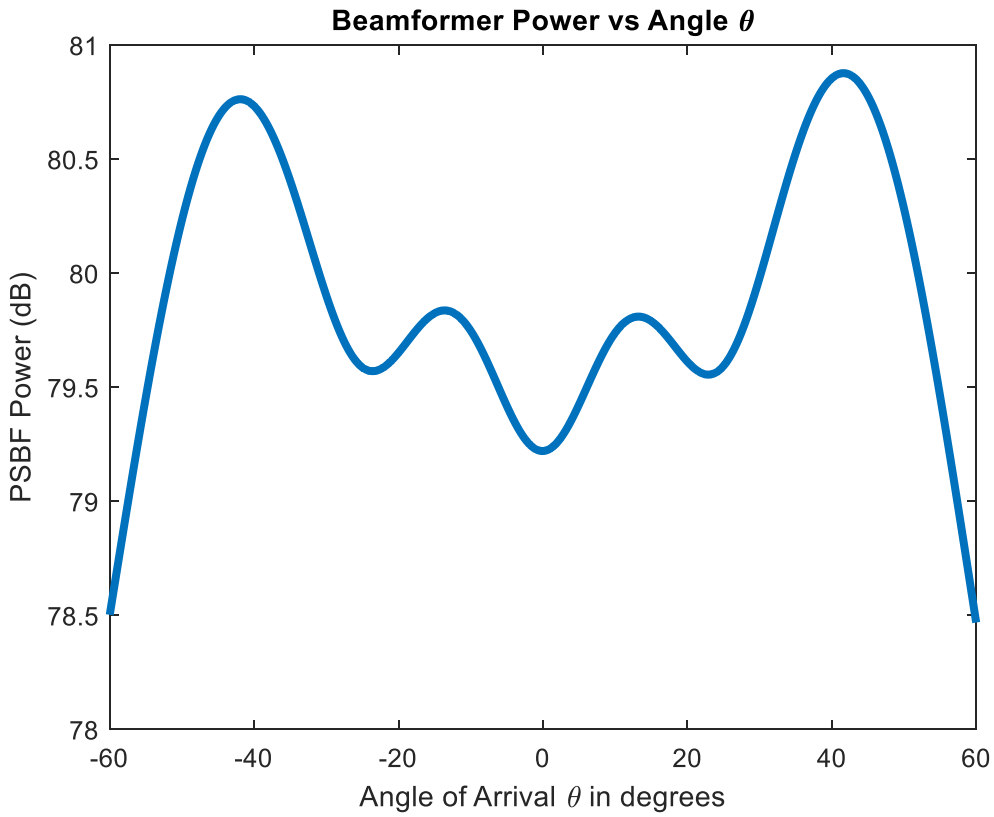

Figure 19. PSBF Output for the Complex Environment Test with Six Sources

The PSBF algorithm shows clear peaks near +/-13, and +/- 42 degrees. The number of sources has caused the system to become underdetermined and no trustworthy measurement can be made. Because the MLE algorithm is an *N-1* dimensional implementation of the PSBF, it is also affected by the same phenomena as the PSBF and therefore it was also unreliable in this scenario.

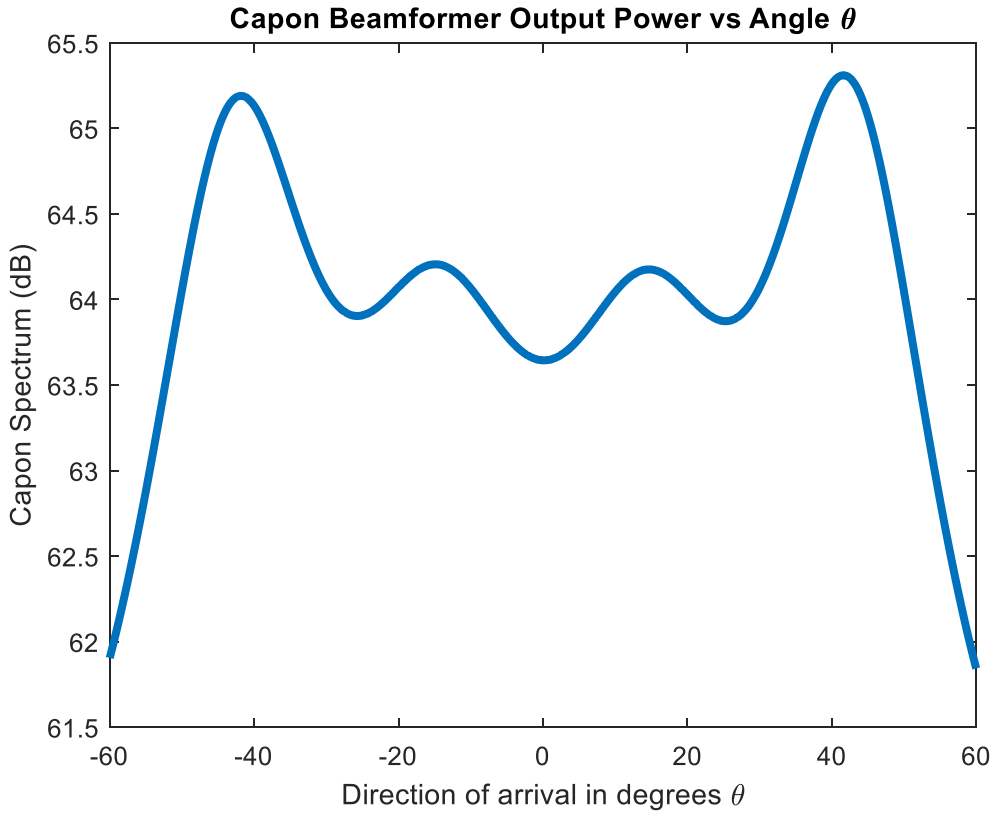

Figure 20. Capon Output for the Complex Environment Test with Six Sources

The Capon beamformer bears a resemblance to the PSBF in Figure 15 that is uncharacteristic of its typical performance. The location of the peaks suggests that no trustworthy measurement can be obtained in this case.

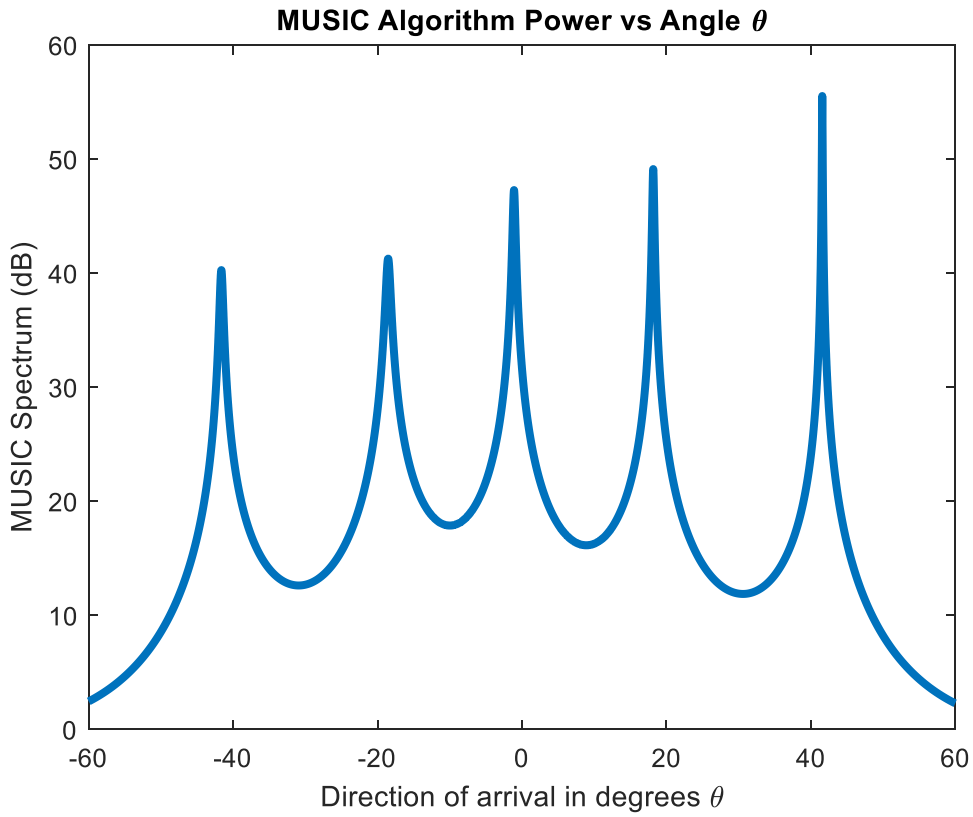

Figure 21. MUSIC Output for the Complex Environment Test with Six Sources

The MUSIC algorithm generates peaks that are characteristic of typical performance however each peak is significantly offset from the actual source and, as expected, no sixth peak is present. This suggest that the MUSIC algorithm is also unreliable in this scenario. This result is expected, recall (37), in the case where six sources are present the noise subspace, U_N, is rank zero – the algorithm as implemented attempts to estimate the noise subspace as rank one, causing algorithm failure.

4.3.6 *Complex Environment Test Summary*

Each algorithm showed capability to detect the AoA of up to five sources in the environment. However, when a sixth source is presented, all algorithms report erroneous

solutions. This is consistent with established bounds on the number of co-channel sources that can be simultaneously located [29].

4.4 Wideband Signal Test

Each of the algorithms operates under the assumption that the signal is narrowband and that the frequency is close to the array manifold's center frequency 1.575 GHz. When this assumption is violated it results in some error in the AoA solution. Since the array manifold, see (6-7), is calculated for the center of the frequency band, a signal that is not centered in the band will have a different phase response across the face of the array than what is anticipated. For example, consider Figure 22.

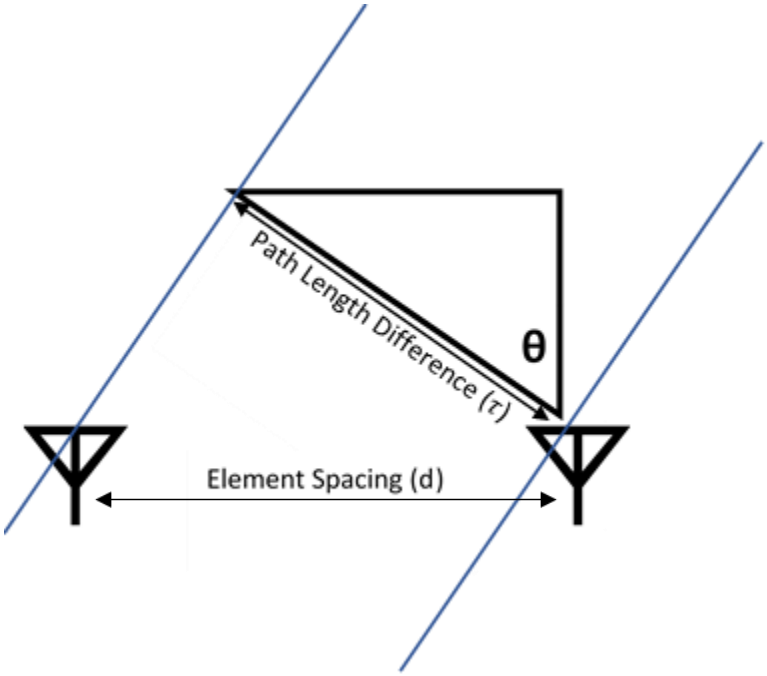

Figure 22. A Plane Wave Incident on Two Elements of a ULA

The blue lines represent two wavefronts from the same signal that are co-incident on the array. The propagation delay between the two wavefronts is given by (40).

$$\tau = \frac{d \sin(\theta)}{c} \tag{40}$$

Recalling the relationship between frequency and phase, the phase difference between the coincident samples of the two antenna elements can be expressed as (41).

$$delta\ phase = \int_0^{\tau} 2\pi f dt = \frac{2\pi d \sin(\theta) f}{c} \tag{41}$$

Since the array manifold is calculated to offset these phase shifts, there is error present when the frequency of the signal does not match the assumption implicit in the array manifold. Considering the parameters FOR and bandwidth of the array used for this research, it is possible to find that the phase error for a signal that is 10 MHz from the center frequency will have a phase error: $|\epsilon_{phase}| = .017$ radians at 60°, which is the edge of the FOR. This phase error corresponds to a maximum angle error: $|\epsilon_{angle}| = .63°$. Therefore, wideband signal error has the potential to drive significant AoA errors; all AoA solutions are ambiguous so long as they are solutions to (42).

$$\sin(\theta_{solution})\, f_{L1} = \sin(\theta_{truth})\, f_{truth} \tag{42}$$

Wideband signal error could be mitigated by measuring the frequency of the incoming signals and adjusting the array manifold; however, in the case where multiple signals are present it may not be possible to assign specific frequencies to each signal. To test the likely impacts of wideband signal error, two tests are constructed: the Frequency Offset Test and the Sawtooth Waveform Test.

4.4.1 *Frequency Offset Test*

In the Frequency Offset Test, each source emits a continuous tone with SNR = 20 dB. The signal parameters and the algorithm AoA results are shown in Table 8.

Table 8. AoA Solutions for a Source with a Frequency Offset

Source	AoA Truth°	f_{center} (MHz)	PSBF°	CAPON°	MUSIC°	MLE°
1	-45	1575+1	-47.9	-45.1	-45.0	-44.9
2	0	L1	-2.6	-0.1	-0.1	0.4
3	45	1575+10	47.0	44.7	44.7	44.9

4.4.2 *Sawtooth Waveform Test*

In the Sawtooth Waveform Test, each source emits a periodic sawtooth swept frequency modulation (FM) waveform that is typical of RF interferers [31]; all sources have SNR = 20 dB. The signal parameters and AoA results for the first test are shown in Table 9 where $f_c = 1575$ MHz.

Table 9. AoA Solutions for Sources Employing RF Jamming Waveforms

Source	AoA Truth°	f_{start} (MHz)	f_{stop} (MHz)	Period (μs)	PSBF°	CAPON°	MUSIC°	MLE°
1	-45	f_c-4.4	f_c+9.6	9	-45.4	-44.6	-44.6	-44.8
2	0	f_c-21.4	f_c+19.6	12	-0.4	0.0	0.0	0.0
3	45	f_c-8.4	f_c+10.6	9	45.3	44.4	44.4	44.6

4.4.3 *Wideband Signal Test Summary*

In the Frequency Offset Test, the algorithms showed the expected susceptibility to AoA error induced by a frequency mismatch with the frequency assumed by the array manifold. Consider source three from the Frequency Offset Test; considering (43) as specific case of (42) it is possible to solve for the expected error in AoA solution for all the algorithms if the true frequency of the signal source is known. Therefore, the AOA error present in the MUSIC and the Capon solutions is expected.

$$\sin(44.7°)\,(f_c) \approx \sin(45°)\,(f_c - 10E6) \tag{43}$$

The larger errors present in the PSBF and MLE methods are very likely due energy entering into the sidelobes of the AoA hypotheses. In the Sawtooth Waveform Test all algorithms performed well and all errors are within |.63|°, as predicted by (40-42).

4.5 Angular Resolution Test

Angular resolution is defined as the ability to accurately measure two closely spaced sources. It has been shown that the angular resolution of the PSBF is approximately equivalent to half of one beamwidth. However, previous findings do not include a restriction on the accuracy of the measurement; only the ability to resolve two individual sources. This research examines how closely two sources can be to one another while calculating AoA to within one degree of error.

For this experiment, two sources with varying SNR are moved closer to one another, in 1° increments, until each algorithm is either unable to measure two individual sources, or the error for the solution exceeds one degree. The first source is held constant at an AoA of

zero degrees while the other source begins at -45 degrees and is moved closer to the first until each algorithm is either unable to resolve the two individual signal sources or the error in the solutions is larger than one degree. Each source radiates a continuous tone near f_c and with a SNR of 20 dB, 30 dB, 40 dB, and infinity. The finest resolution achieved by each algorithm before failure at each SNR is reported in Table 10.

Table 10. Angular Resolution Test Results

Algorithm	SNR = 20 dB	SNR = 30 dB	SNR = 40 dB	SNR = Inf.
PSBF	20°	19°	19°	19°
Capon	7°	3°	3°	1°
MUSIC	3°	1°	1°	1°
MLE	19°	17°	17°	17°

4.5.1 *Angular Resolution Test Summary*

The results show that the PSPF and MLE methods are far less capable of fine AoA resolution than Capon and MUSIC. Considering the results as a function of SNR it is clear that with high SNR the PSBF algorithm's resolution approaches 19°, which is approximately one-half of the beamwidth of the mainbeam for the array. The beampattern for the antenna pointing a beam at zero degrees azimuth is shown in Figure 23.

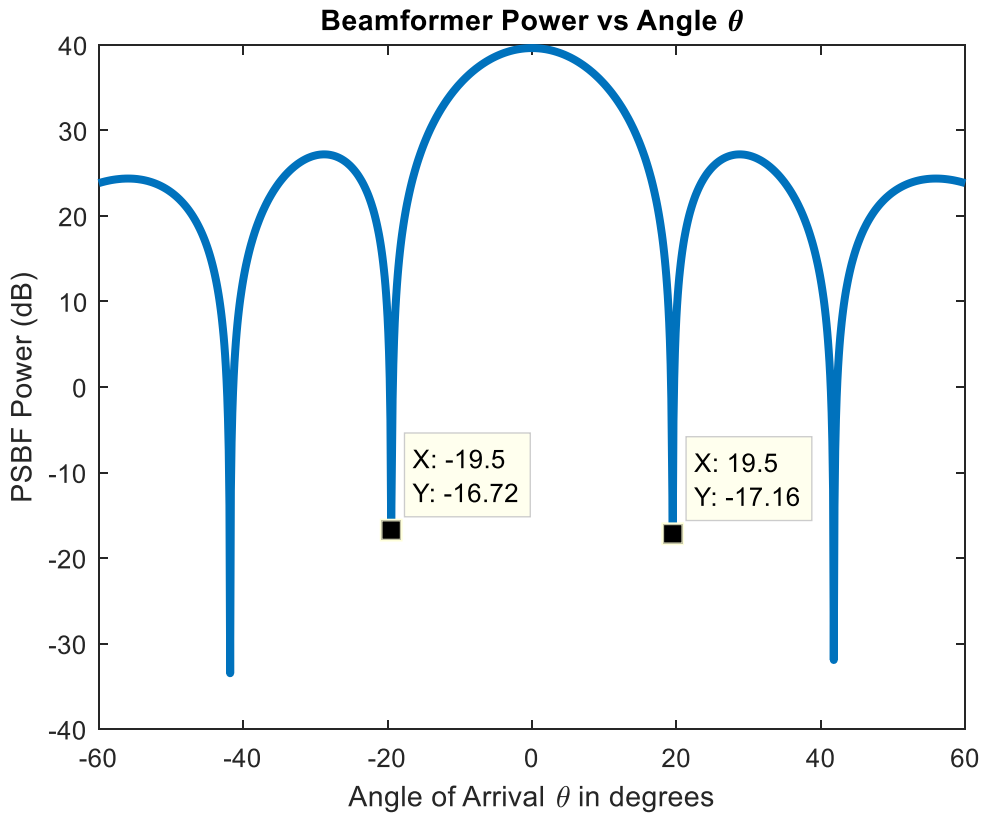

Figure 23. Antenna Pattern for a Beam Steered to Zero Degrees

It is interesting that the MLE algorithm is able to improve on this result slightly with an AoA resolution that approaches 17° at high SNR levels. The results for Capon and MUSIC show that they approach one degree of AoA accuracy when SNR is high, with MUSIC outperforming Capon at any given SNR. These results are consistent with the findings in a previous study [28].

4.6 Coherent Source Test

A known issue with passive AoA systems is spatially distributed, phase-coherent sources. In the event that two coherent wavefronts are present on the antenna, the wavefronts

combine to produce one wavefront potentially rendering all of the studied algorithms ineffective.

To test the vulnerability of coherent sources this study asks the question “How coherent must the sources be to defeat passive AoA”? For the Coherent Sources Test, two sources radiating the same waveform are inserted into the environment with some offset in their center frequency. This frequency offset is reduced until each algorithm fails to resolve the individual sources.

4.6.1 *Coherent Sources Test Results*

This test found that a frequency offset as little as 1 Hz is sufficient to enable AoA solutions from every algorithm. However, it does degrade algorithm performance as the offsets are reduced. Figure 24 shows the output of the MUSIC algorithm when the frequency offsets are 10 kHz, 1 kHz, 1 Hz, and zero.

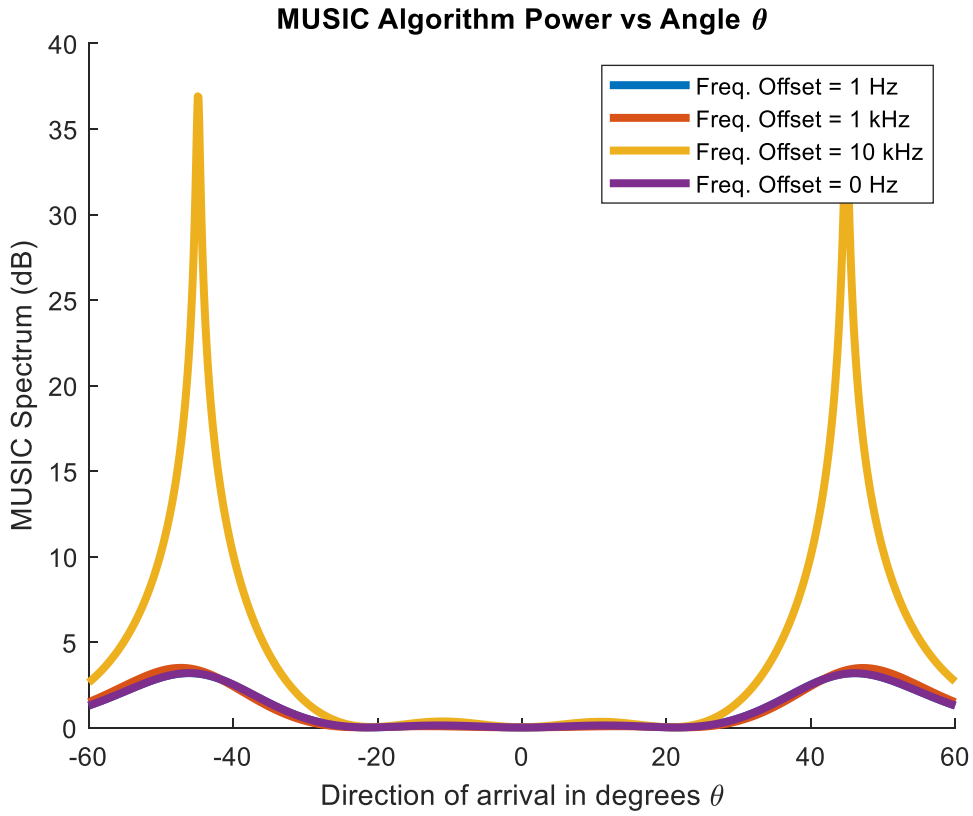

Figure 24. AoA Results for Two Coherent Sources

Clearly as the two sources approach one-another in frequency the algorithm performance degrades. The reduced height of the peaks peak below 10 kHz suggests that the algorithm will have reduced dynamic range, and may not perform well at low SNR levels when spatially distributed coherent sources are present.

Note that this applies only to sources that are "phase locked" or approaching a phase lock. Sources that are not correlated in phase but possess complex, overlapping frequency spectra are tested in the Wideband Signal Test and did not significantly degrade algorithm performance. This result is consistent with previous findings for the MUSIC algorithm.

Some implementations of the MLE and MUSIC algorithm are reportedly able to better deal with coherent signal sources [3], however due the to technical difficulty in achieving a phase-lock between two spatially diverse signal sources this thesis does not study the issue any further.

4.7 Antenna Position Error Monte' Carlo

In practice every array is calibrated. Typically, this includes physical measurement of the array manifold, as opposed to idealized calculation presented in Section II. After one article is measured it is desirable to apply this calibration to other identical units, thus eliminating the need for robust calibration on every individual sensor unit. This calibration always involves some error. This error may be from many sources including differences in electrical properties of the components used, thermal expansion of the antenna itself, or manufacturing accuracy limitations in the placement of the antenna radiators creating errors in the distances between elements. Ultimately, these phenomena introduce variation from the calibration that cause errors in the AoA solution.

To study these errors a Monte` Carlo simulation examines the effect of erroneous antenna phase center locations. The ideal antenna placements are varied by a random, gaussian, zero-mean error term in three dimensions as described in (43) where $Antenna_x$, $Antenna_y$, and $Antenna_z$ are the true locations of each antenna element and $\epsilon_X, \epsilon_Y, \epsilon_Z$ are the error terms.

$$[Antenna_X, Antenna_Y, Antenna_Z] + [\epsilon_X, \epsilon_Y, \epsilon_Z] \tag{43}$$

The standard deviation of $\epsilon_X, \epsilon_Y,$ and ϵ_Z is increased from 1 mm to 30 mm, and 100 runs are accomplished at each standard deviation. For every set of random errors, each AoA algorithm calculates the AoA to three ideal sources located at 45, 0, and -30 degrees in the FOR. The outputs of this study are the error mean, error standard deviation and the algorithm failure rate. Algorithm failure is considered to have occurred if the algorithm reports too many or too few sources in the environment. When an algorithm failure occurs, the AoA results for that run are thrown out and are not used to calculate the error mean or standard deviation. For this research an algorithm is considered robust to a level of calibration error so long as its algorithm failure rate remains below fifty percent and its mean error is below one degree. All three sources have 40 dB SNR.

4.7.1 *Antenna Position Error Monte' Carlo Results*

The PSBF results are shown in Figure 25.

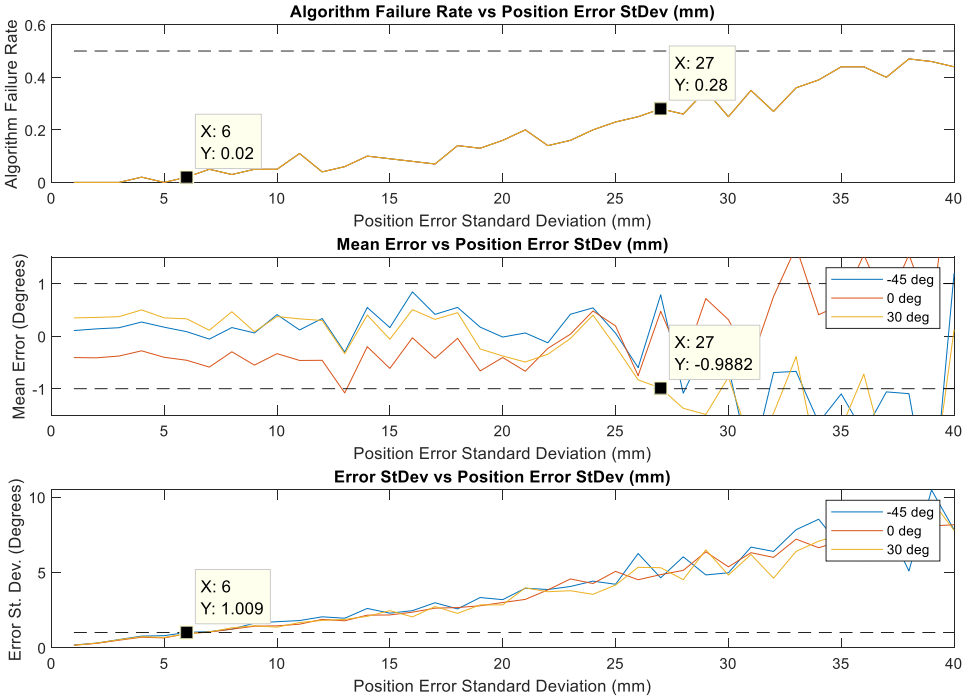

Figure 25. PSBF Antenna Position Error Monte' Carlo Results

The failure mode for PSBF is mean error greater than one degree. Failure occurs at error standard deviations greater than 27 mm; algorithm failure rate is 28% at this level. AoA error standard deviation exceeds one degree at position error standard deviation levels greater than 6 mm; algorithm failure rate is 2% at this level. The Capon results are shown in Figure 26.

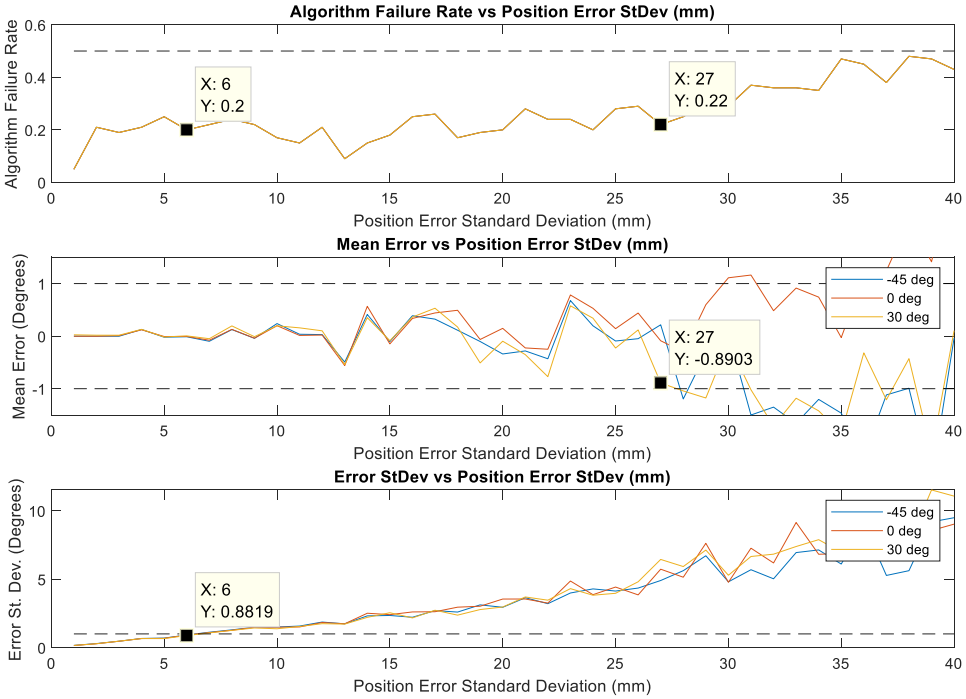

Figure 26. Capon Antenna Position Error Monte' Carlo Results

The failure mode for Capon is mean error greater than one degree. Failure occurred at error standard deviations greater than 27 mm; algorithm failure rate is 22% at this level. AoA error standard deviation exceeded one degree at position error standard deviation levels greater than 6 mm; algorithm failure rate was 20% at this level. The MUSIC results are shown in Figure 27.

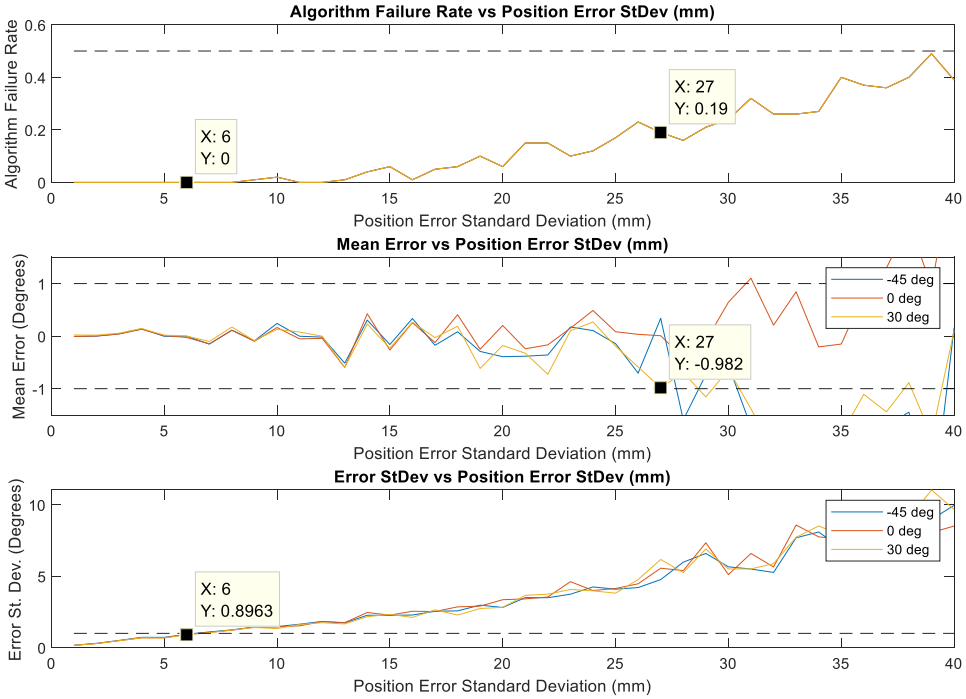

Figure 27. MUSIC Antenna Position Error Monte' Carlo Results

The failure mode for MUSIC was mean error greater than one degree. Failure occurred at error standard deviations greater than 27 mm, algorithm failure rate was 19% at this level. AoA error standard deviation exceeded one degree at position error standard deviation levels greater than 6 mm, algorithm failure rate was 5% at this level.

The MLE results are shown in Figure 28.

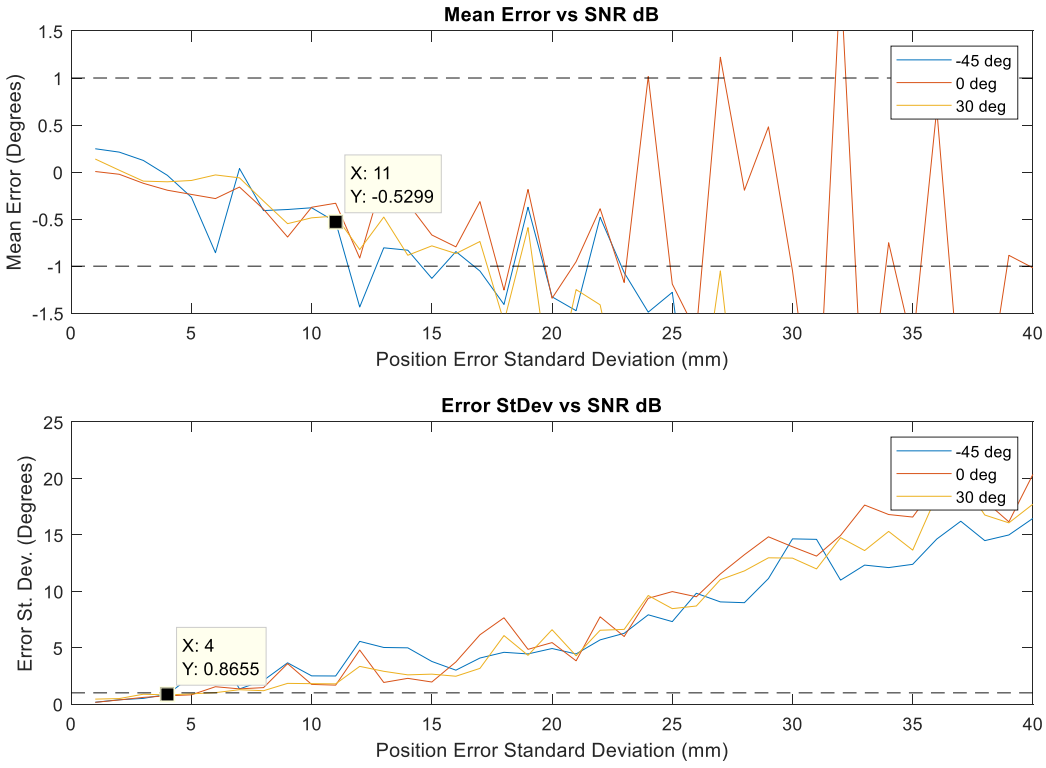

Figure 28. MLE Antenna Position Error Monte' Carlo Results

Failure occurred at error standard deviations greater than 11 mm. AoA error standard deviation exceeded one degree at position error standard deviation levels greater than 4 mm.

4.8 Phase Calibration Error Monte' Carlo

In practice each receiver chain is independently calibrated to match its phase response to the others; however, there is always residual error present. This test measures the AoA error as a function of error in the phase calibration of the array. For this simulation an error term is applied to each antenna in the receive array; the error term is constant for every sample of each antenna. Equation (44) shows the alteration to the sampling matrix

used for this test where each ϵ is a zero-mean, Gaussian random variable between 0 and 2π, and $times(\quad)$ is the element-wise multiplication function.

$$X_{sample+phase\ error} = times\left(X_{sample\ clean}, \begin{bmatrix} e^{i\epsilon_1} \\ \vdots \\ e^{i\epsilon_N} \end{bmatrix}\right) \tag{44}$$

The standard deviation of the error, ϵ, terms is treated as the independent variable and the AoA solutions from each algorithm are treated as dependent variables. Three sources are present in the environment and are located at 45, 0, and -30 degrees. All three sources have 40 dB SNR. The outputs of this simulation are mean error, error standard deviation, and algorithm failure rate.

4.8.1 *Phase Error Calibration Results.*

The results for the PSBF algorithm are shown in Figure 29.

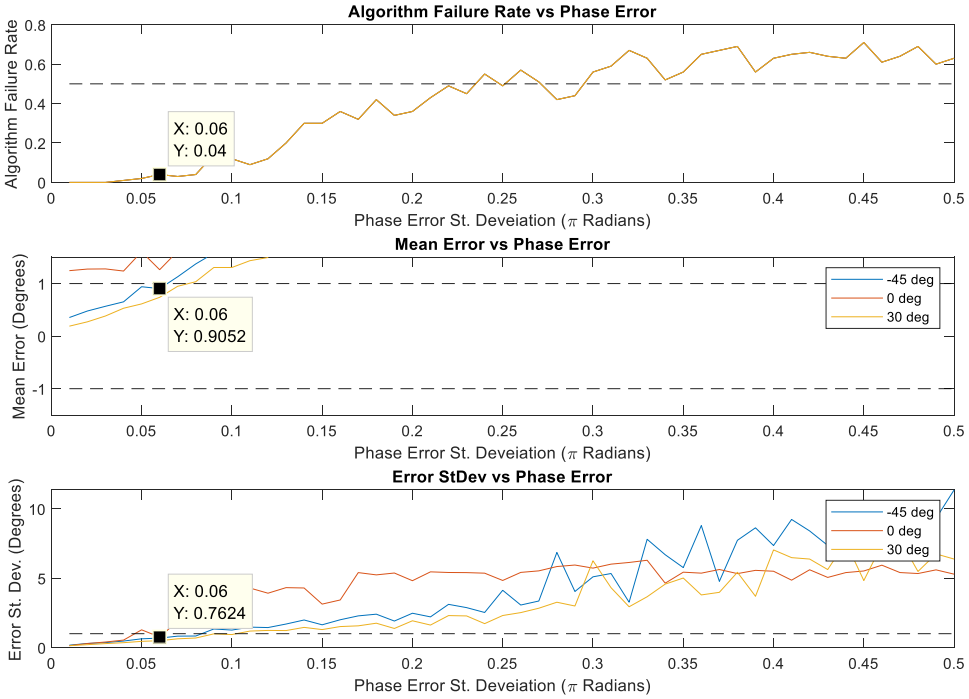

Figure 29. PSBF Phase Calibration Error Monte' Carlo Results

The failure mode for the PSBF algorithm was mean error greater than one degree. Failure occurred at error standard deviations greater than .06π radians. AoA error standard deviation also exceeded one degree at phase error standard deviation levels greater than .06π radians, algorithm failure rate was 4% at this level. The results for the Capon beamformer are shown in Figure 30.

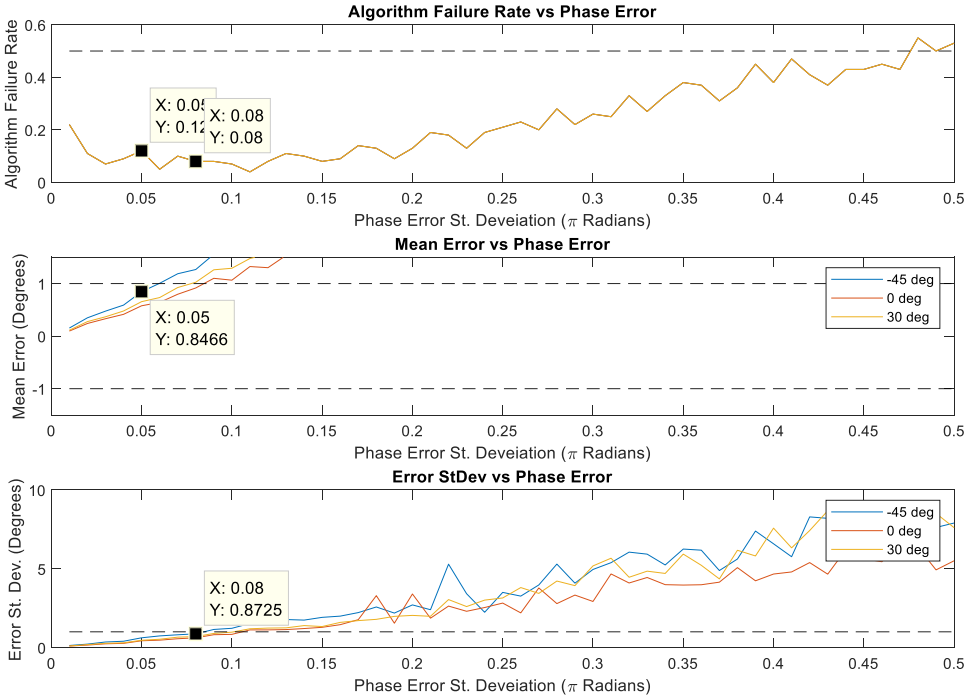

Figure 30. Capon Phase Calibration Error Monte' Carlo Results

The failure mode for the Capon algorithm was mean error greater than one degree. Failure occurred at error standard deviations greater than .05π radians, algorithm failure rate was 12% at this level. AoA error standard deviation exceeded one degree at position error standard deviation levels greater than .08π radians, algorithm failure rate was 8% at this level. The results for the MUSIC algorithm are shown in Figure 31.

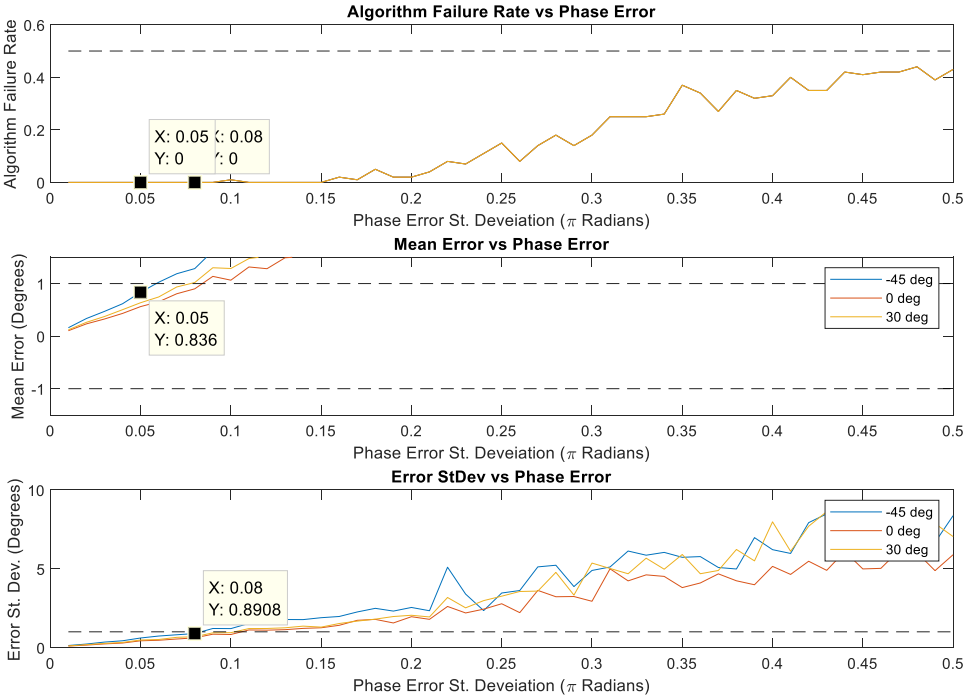

Figure 31. MUSIC Phase Calibration Error Monte' Carlo Results

The failure mode for the MUSIC algorithm was mean error greater than one degree. Failure occurred at error standard deviations greater than .05π radians, algorithm failure rate was 0% at this level. AoA error standard deviation exceeded one degree at position error standard deviation levels greater than .08π radians, algorithm failure rate was 0% at this level. The results for the MLE algorithm are shown in Figure 32.

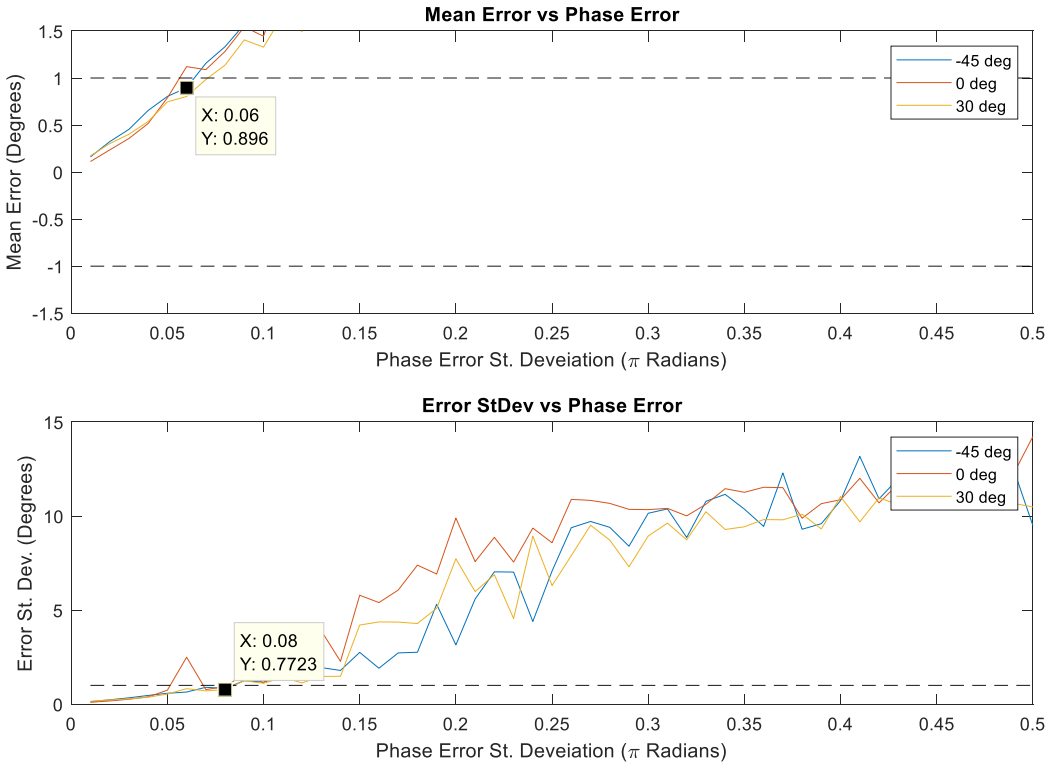

Figure 32. MLE Phase Calibration Error Monte' Carlo Results

Failure occurred at error standard deviations greater than .08π radians. AoA error standard deviation exceeded one degree at position error standard deviation levels greater than .08π radians.

4.9 Multipath Interferer Monte' Carlo

This test studies each algorithms' response to multipath interference in the environment. Two multipath interference sources are introduced into the environment. Each source in placed at a random location in a $20 \times 20\ km^2$ box in front of the antenna. The multipath interferers reflect the signal from each interference source with a random phase shift that

is different for each source. In this test the power of the multipath signal is treated as the independent variable; the locations of the interferers are random variables, the phase shift for each source is a random variable, and the AoA solutions are the dependent variables. The results are presented as a function of multipath to direct path ratio (M/D) which is defined according to (45).

$$\frac{M}{D}(dB) = 20\log_{10}(\frac{Multipath\ Volatage}{Source\ Signal\ Voltage}) \quad (45)$$

The power of each multipath interferer varies from -40 dB to -6 dB with respect to the power of the sources. One hundred runs are accomplished at each power level and the error mean, error standard deviation, and algorithm failure rates are reported.

4.9.1 *Multipath Interferer Monte' Carlo Results*

The results for the PSBF are shown in Figure 33.

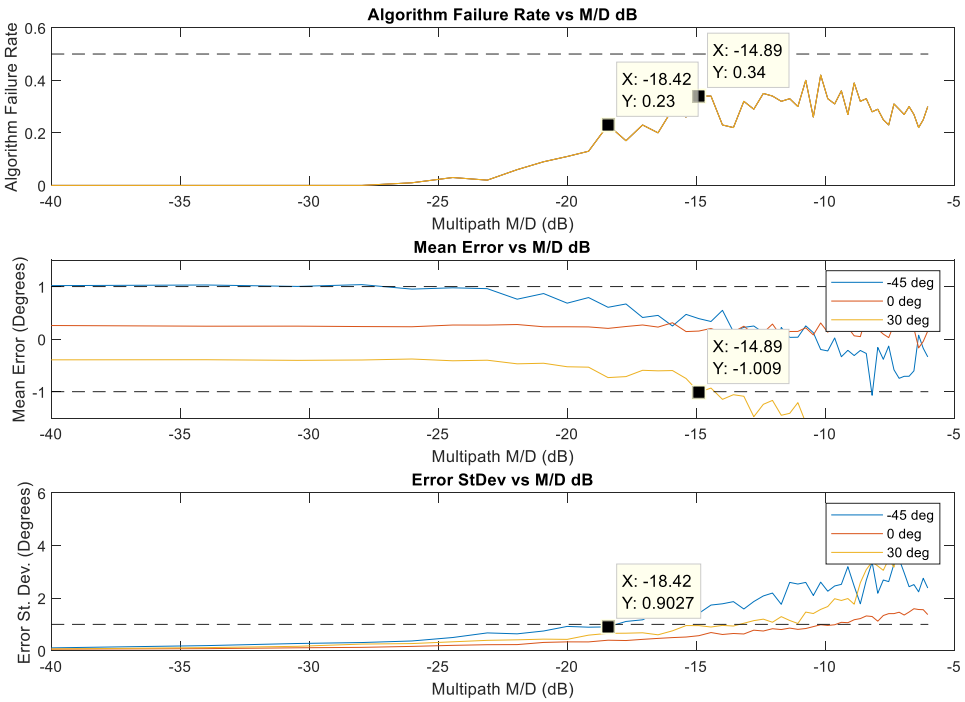

Figure 33. PSBF Multipath Interferer Monte' Carlo Results

Mean error greater than one degree is the failure mode for the PSBF. Failure occurs at M/D ratios greater than -14.89 dB, algorithm failure rate was 34% at this level. AoA error standard deviation exceeds one degree at M/D ratios greater than -18.42 dB, algorithm failure rate was 23% at this level. The results for the Capon algorithm are shown in Figure 34.

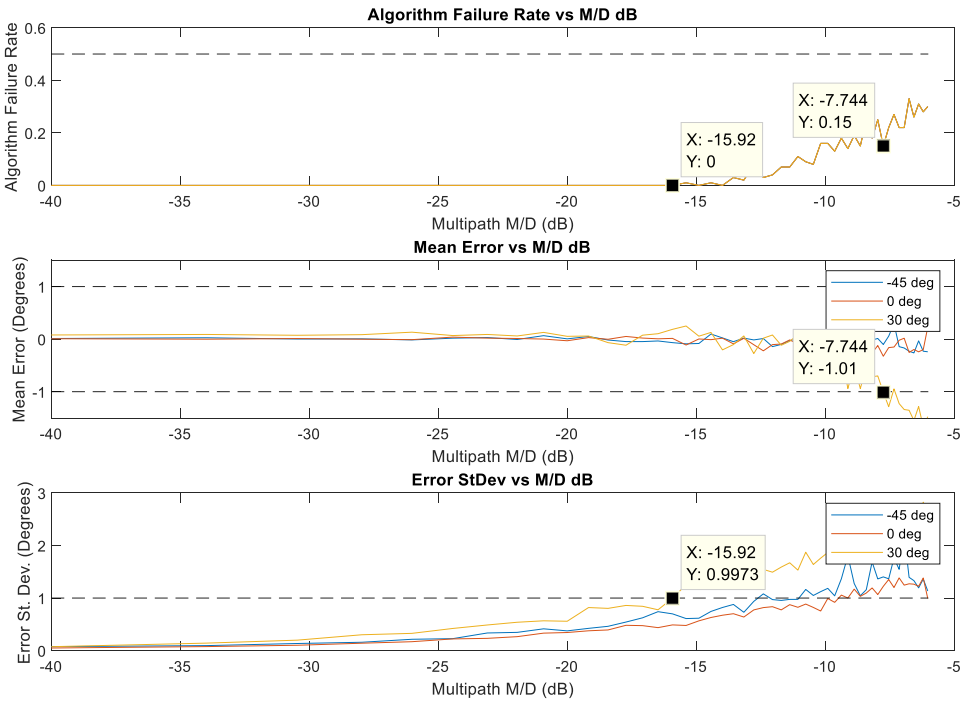

Figure 34. Capon Multipath Interferer Monte' Carlo Results

Mean error greater than one degree is the failure mode for the Capon algorithm. Failure occurs at M/D ratios greater than -15.9 dB, algorithm failure rate was 0% at this level. AoA error standard deviation exceeds one degree at M/D ratios greater than -7.7 dB, algorithm failure rate is 15% at this level. The results for the MUSIC algorithm are shown in Figure 35.

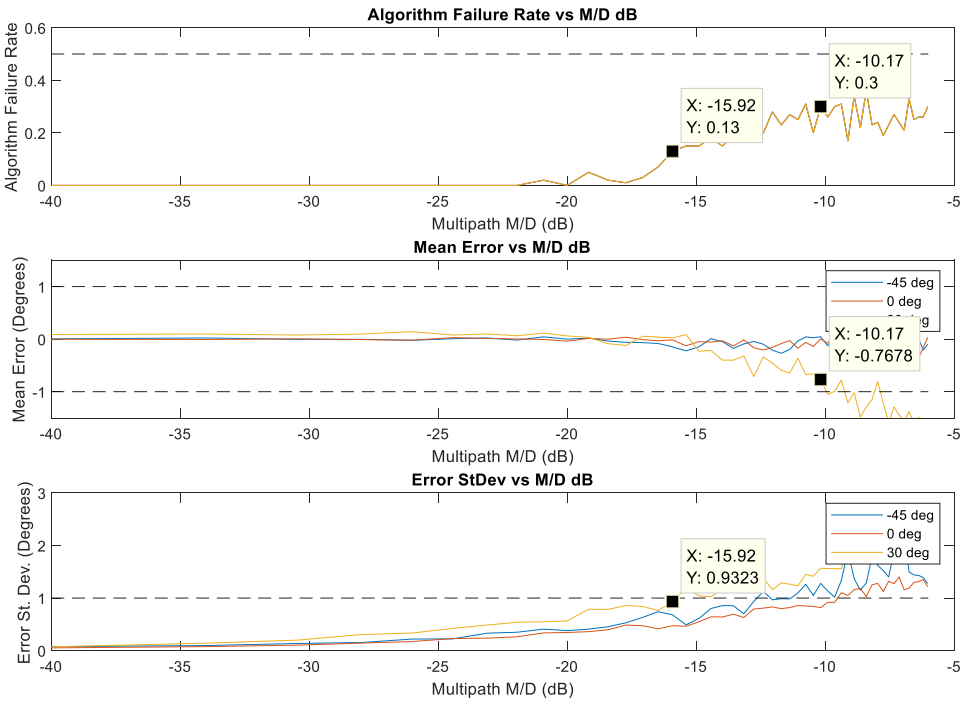

Figure 35. MUSIC Multipath Interferer Monte' Carlo Results

Mean error greater than one degree is the failure mode for the Capon algorithm. Failure occurs at M/D ratios greater than -10.2 dB, algorithm failure rate is 30% at this level. AoA error standard deviation exceeds one degree at M/D ratios greater than -15.9 dB, algorithm failure rate is 13% at this level. The results for the MLE algorithm are shown in Figure 36.

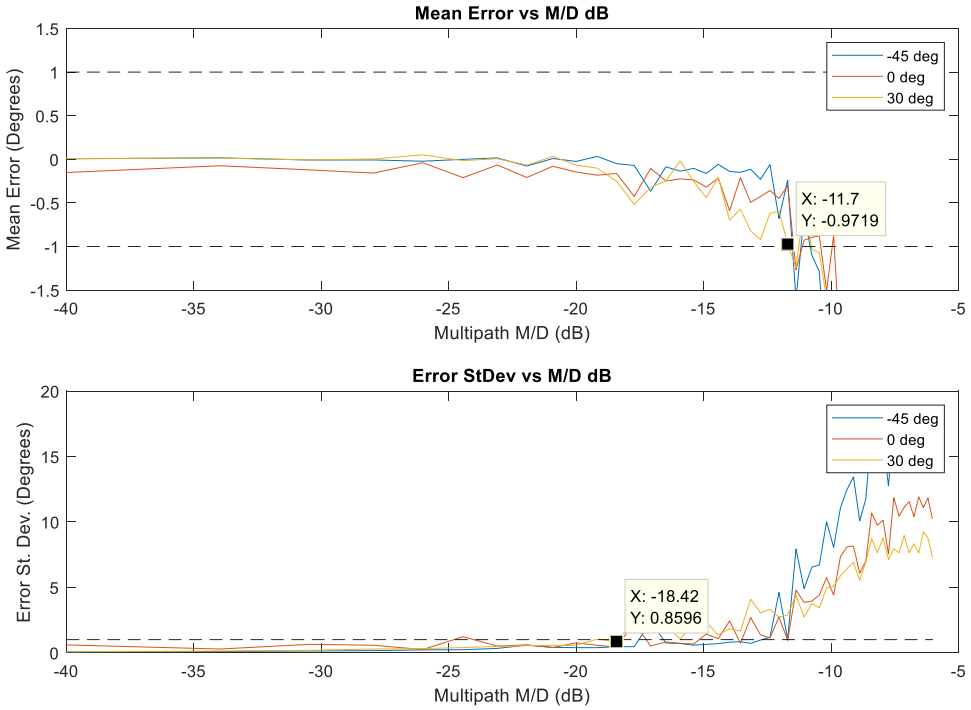

Figure 36. MLE Multipath Interferer Monte' Carlo Results

Failure occurred at M/D ratios greater than -11.7 dB. Error standard deviation occurred at M/D ratios greater than -18.4 dB.

4.10 Instantaneous Dynamic Range Monte' Carlo

To determine each algorithms' dynamic range a Monte` Carlo simulation is accomplished. Noise power level is held steady at -20 dB relative to the smallest signal in the environment. Two signals are present in the environment, the second signal in the environment is introduced with a signal power that varies from 0 to 20 dB relative to the first signal. Each dynamic range level is simulated 100 times. Dynamic range is calculated according to (46).

$$Dynamic\ Range\ (dB) = 20 \log \left(\frac{Source1\ Amplitude}{Source2\ Amplitude} \right) \quad (46)$$

The outputs of this study are the error mean, error standard deviation and the algorithm failure rate. For this research, an algorithm is considered usable at a given dynamic range so long as its algorithm failure rate remains below fifty percent.

4.10.1 *Instantaneous Dynamic Range Results*

The results for the PSBF are shown in Figure 37.

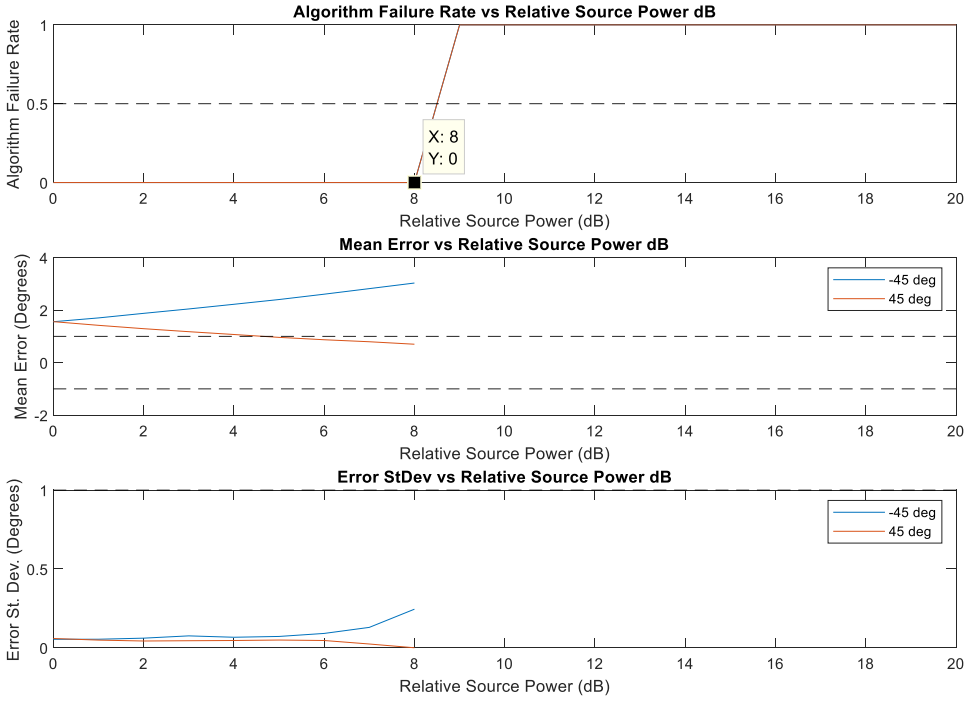

Figure 37. PSBF Instantaneous Dynamic Range Monte` Carlo Results

The PSBF has an instantaneous dynamic range of 8 dB. In practice the dynamic range of the PSBF is determined by the algorithm implementation, in this case the threshold for detection was any signal greater than –9 dB from the main peak; this threshold was used

to attempt to limit false detections the coherent addition of sidelobes that is shown in Figure 12. The results for the Capon beamformer are shown in Figure 38.

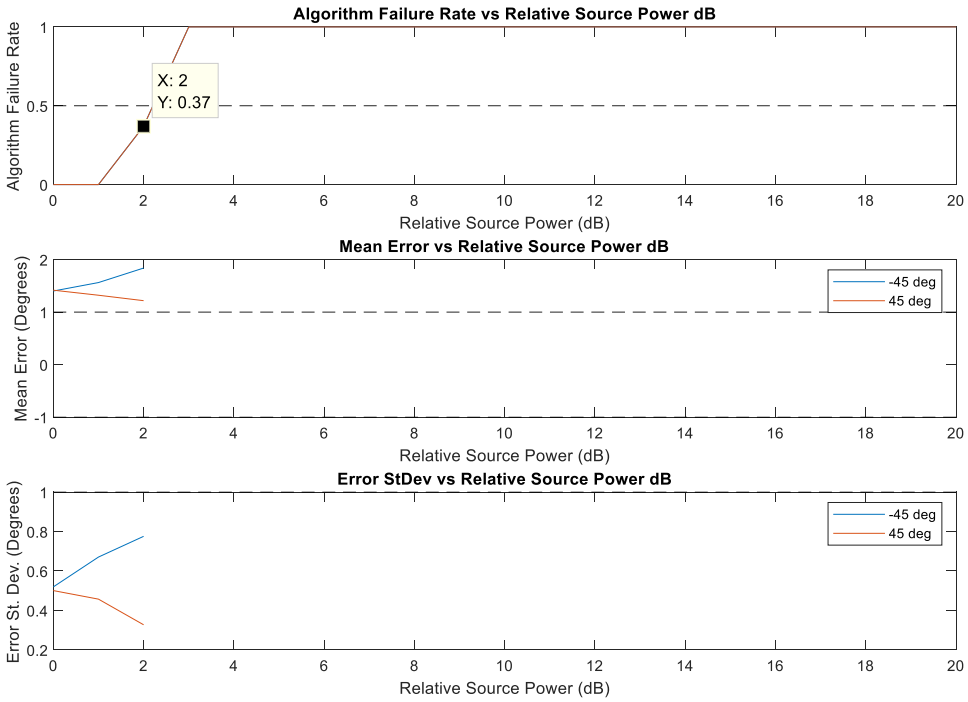

Figure 38. Capon Instantaneous Dynamic Range Monte` Carlo Results

The Capon algorithm has an instantaneous dynamic range of only 2 dB. This is due to the fact that a second strong source in the environment is always raising the effective noise floor of the algorithm when the null is not steered in its direction. This phenomenon desensitizes the Capon algorithm making it unable to find sources that are significantly weaker than the strongest source in the environment. The results for MUSIC are shown in Figure 39.

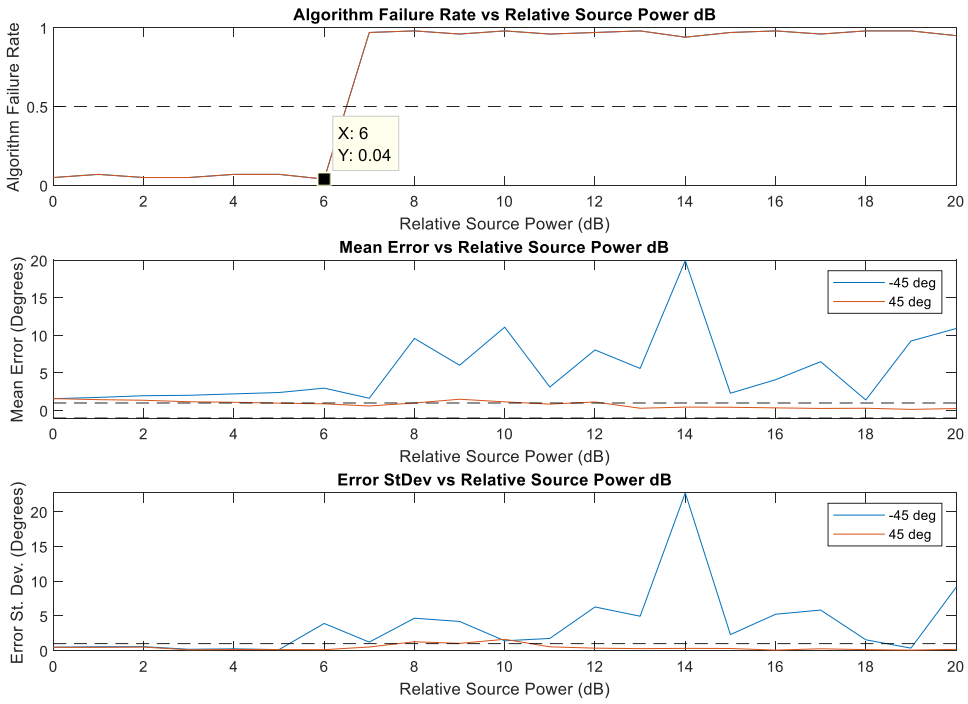

Figure 39. MUSIC Instantaneous Dynamic Range Monte` Carlo Results

The MUSIC algorithm has an instantaneous dynamic range of 6 dB. So long as the eigenvalues of the signal subspace are significantly larger than those from the noise subspace MUSIC is able to detect both sources. The results for MLE are shown in Figure 40.

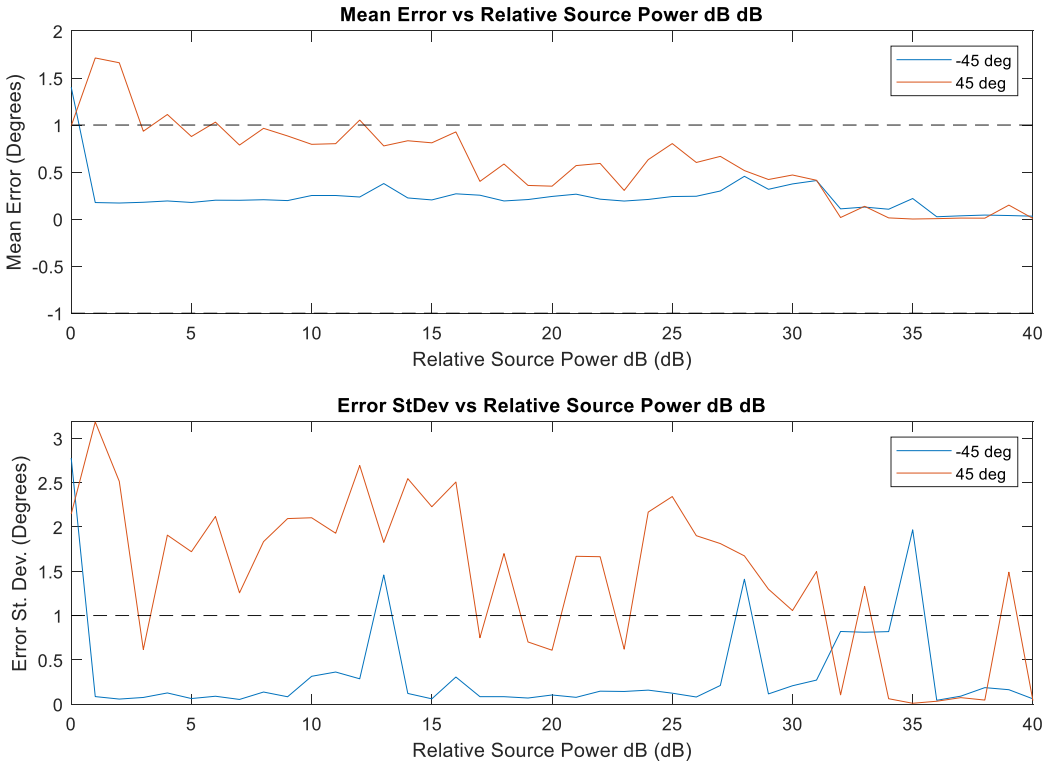

Figure 40. MLE Instantaneous Dynamic Range Monte` Carlo Results

The MLE algorithm shows instantaneous dynamic range through 20 dB so the experiment is extended to test dynamic range through 40 dB. The outstanding performance of the MLE algorithm is due to its iterative nature. Even if the weaker source exists below the sidelobes of the stronger source the algorithm will an additional beam at the weaker source, thus changing the sidelobe structure and revealing the second source. These simulations show that the MLE algorithm is exceptional at sorting through the FOR to find additional sources even when they are much weaker than the strongest signal in the environment.

V. Conclusion

This section recaps the goals of the research, summarizes and briefly comments on the results, and offers an algorithm recommendation for an angle-of-arrival (AoA) algorithm to radiofrequency (RF) interferers.

5.1 Algorithm Results Summary

The first goal of this research was to examine AoA methods in the context of real-world challenges to algorithm performance. Four AoA algorithms were studied in this effort:

- The Phase-shift Beamformer (PSBF)
- The Capon or Minimum Variance Distortionless Response (MVDR) beamformer
- The Multiple Signal Identification and Classification (MUSIC) algorithm
- The Maximum Likelihood Estimation (MLE) algorithm

Each algorithm was examined to characterize the computation burden of each method. All of the closed-form solutions: MUSIC, PSBF and Capon, had similar computational burdens. However, MLE, since it is an iterative algorithm, had a computational burden that was 1-2 orders of magnitude greater than the other methods.

The performance of each of these algorithms was studied in the presence of non-ideal conditions. The conditions studied were:

- Cluttered signal environments
- Wideband signals
- Closely-spaced signal sources

- Spatially-diverse, phase-coherent sources
- Antenna manufacturing errors
- Phase calibration errors
- Low signal-to-noise ratio (SNR)
- Strong multipath interferers
- Signal sources with large differences in signal power (Instantaneous Dynamic Range)

To accomplish the study a modeling and simulation (M&S) environment was developed using MATLAB™. The M&S environment models the radio frequency signal environment from the antenna, through mixing, filtering and analog to digital conversion where the data can then be presented to the AoA algorithms for processing. Table 11 ranks algorithm performance in each test from one to four, one being the best.

Table 11. AoA Algorithm Results Rankings

Test	PSBF	Capon	MUSIC	MLE
Complex Environment	4	1 (tie)	1 (tie)	3
Wideband Signals	4	1	2	3
Angular Resolution	4	2	1	3
Phase Coherent Sources	1 (tie)	1 (tie)	1 (tie)	1 (tie)
Antenna Position Errors	2	4	1	3
Phase Calibration Errors	2	4	3	1
SNR	2	3	4	1
Multipath Interference	4	1	2	3
Instantaneous Dynamic Range	2	4	3	1

This table, broadly agrees with previous work on the topic [3]. The notable exception is the MLE algorithm, which does not achieve the best result in every category as some literature would predict, this is certainly due to the implementation chosen for this thesis which exchanged the exhaustive MLE techniques for a faster implementation that is more susceptible to errors but has reduced computational costs [30]. A few results deserve

some discussion. The angular resolution of the destructive interference methods, MUSIC and Capon, were one degree with sufficient SNR; this is a very large improvement over the constructive interference methods, PSBF and MLE. The MLE method was by far the best method for finding signals with significantly different power levels; it was able to detect two signals with 40 dB difference in their power levels. The next best-performing method was PSBF with 8 dB of instantaneous dynamic range.

5.2 Algorithm Recommendations

The second goal for this research was to determine the best algorithm for determining the AoA of RF interferers in civilian and military applications. For applications where the number of RF interferers is likely to be low, the MUSIC technique is best suited. Examination of the results in Table 11 and the computational complexity analysis in Section 3.3 suggests that, assuming a serial algorithm implementation, a hybridized algorithm would be equally effective as MUSIC while being more computationally efficient. The hybridized algorithm runs in two stages. The first stage uses a coarse PSBF algorithm where the AoA hypothesis is applied every 5°. When a signal source is detected that region will be searched more finely by the second stage. The second stage of the hybridized algorithm is the MUSIC algorithm with an AoA resolution of .1°. This algorithm is a carefully constructed implementation of a derivative of the MUSIC algorithm known as Beamspace MUSIC when it is carefully tailored to the characteristics of the available ULA [3]. Figure 41 shows a flow chart of the hybrid algorithm with the number of operations for each stage shown.

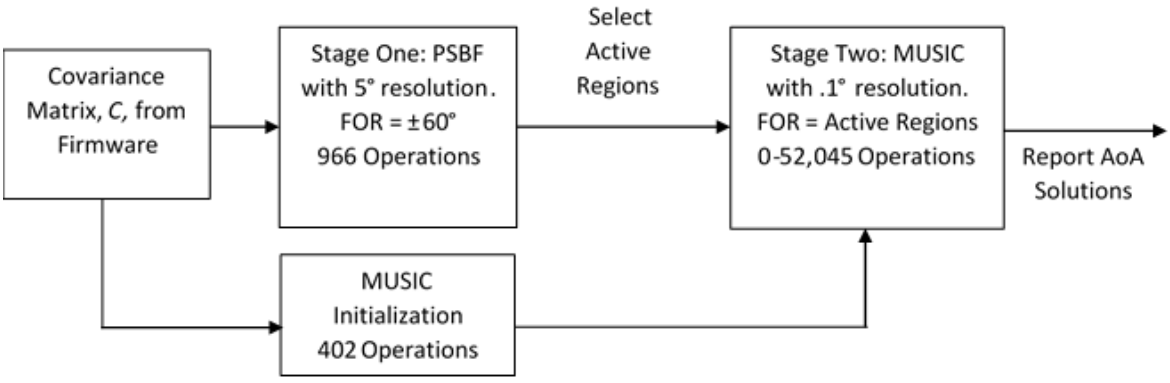

Figure 41. Hybrid Algorithm Flowchart

Because the PSBF algorithm has better dynamic range and low SNR performance than the MUSIC algorithm, no performance is lost by using it as the initial detection stage so long as the resolution is not so coarse that the beam is significantly off-target of the signal source. In this case 5° resolution was chosen because it is within the 3dB beamwidth of the array.

Once the first-stage algorithm detects the possibility of a signal in a region of the field of regard (FOR), that region is scanned by the second-stage algorithm. The second stage uses the MUSIC algorithm to optimize accuracy and resolution of the final AoA measurements. In cases where there is only one source in the environment the computational advantage of the hybrid algorithm compared to the MUSIC algorithm is greatest, while in more complex scenarios the advantage will be reduced.

Consider the case where one source is present in the environment at -3.5°. The first stage reports a detection at -5°. This initial detection narrows the FOR searched by the second stage to: -25° - +15°. The size of the FOR in this case is driven by the Angular Resolution

Test in Section 4.4 which shows that the PSBF has an angular of resolution ±20°. Figure 42 shows the output of the first stage of the algorithm.

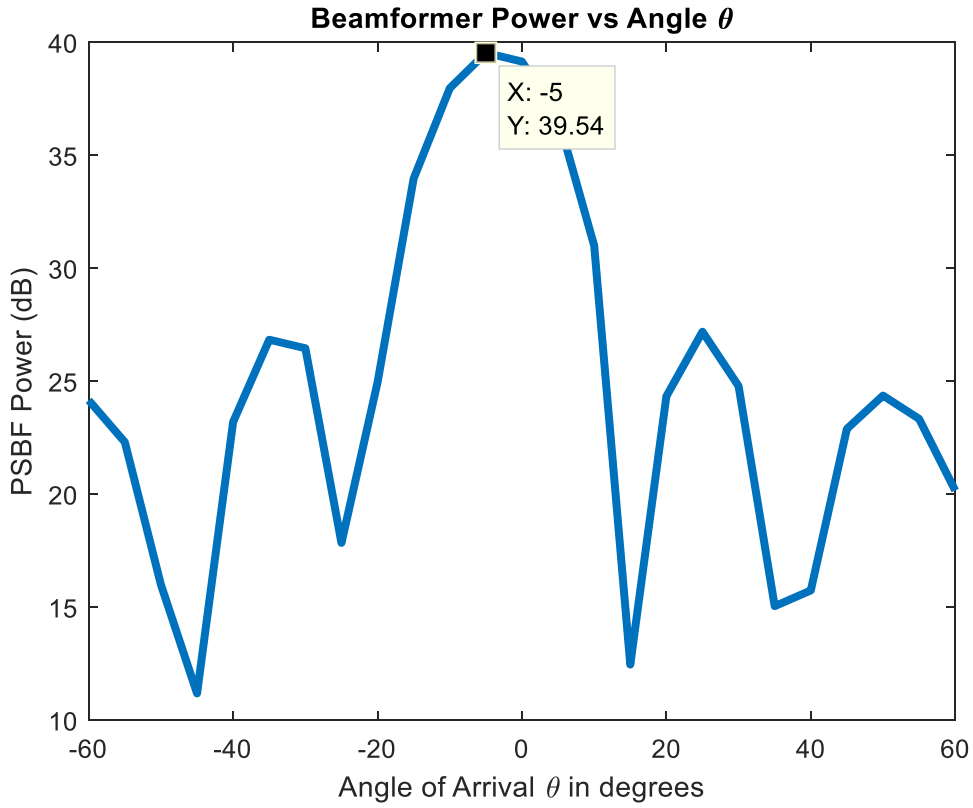

Figure 42. First Stage Hybrid Algorithm Output for a Source at -3.5°

Next, the second stage operates over the narrowed FOR, the output of the second stage is shown in Figure 43.

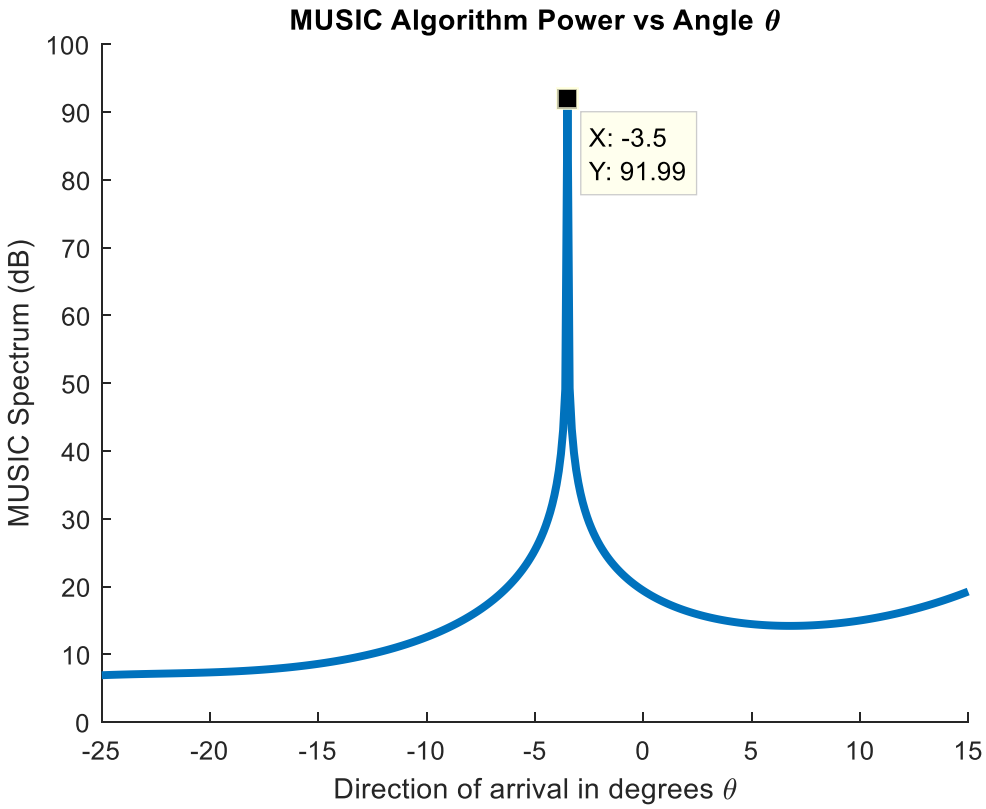

Figure 43. Second Stage Hybrid Algorithm Output for a Source at -3.5°

In this second stage the resolution and accuracy of the MUSIC algorithm is achieved at greatly reduced computational cost. The first stage required 966 operations and the second stage required 17,243 operations for a total of 18,209 operations. Recall Section 3.3 where the computational cost of the MUSIC algorithm over the entire FOR with .1° angular resolution was calculated to require 52,045 operations. Hence, in this case, the hybrid algorithm reduced computational burden by 65% when compared to the MUSIC algorithm while retaining the performance of the MUSIC algorithm.

Alternatively, consider the computational burden of the worst-case scenario where the first stage fails to narrow the FOR and the second stage requires the full cost of the MUSIC algorithm (i.e. 52,045 operations), in addition to the 966 operations spent in the first stage.

In this case the computational burden is increased by 1.9% relative to the full MUSIC algorithm.

The final case to consider is one where instantaneous dynamic range of the sensor is the most important consideration. In this case the MLE algorithm should be used since it significantly outperformed the closed-form algorithms when multiple signal sources had significantly different power levels.

5.3 Summary

This research has examined AoA algorithms for the purpose of locating RF interference sources using a ULA. Four AoA algorithms were compared for performance in the presence of error sources when implemented on an existing sensor. Altogether the simulation results show the sensitivity of AoA estimation systems to sources of error. These results can be used to better estimate the performance of AoA measurement systems in challenging conditions.

Algorithm recommendations were made, subject to system requirements. Using the results of the performance analysis, an optimized hybrid algorithm that makes use of the desirable attributes of the PSBF and MUSIC algorithms was presented. The hybrid algorithm retains the performance characteristics of the MUSIC algorithm but with a reduced computational cost.

Bibliography

[1] S. Xu, S. Wang, C. Han & J. Ma, "Angular Strobe and Tracking of Jammers for Passive Monopulse Seeker," in *2006 CIE International Conference on Radar*, Shanghai, 2006.

[2] D. Price and M. Bartett, "Digital Beamforming for Adaptive Antennas in Mobile Communications: Practical Results from Super Resolution Direction Finding Methods," Institue of Electrical Engineers, London, 1994.

[3] H. Krim and M. Viberg, "Two Decades of Array Signal Processing Research," *IEEE Signal Processing Magazine,* vol. 13, no. 4, pp. 67-94, 1996.

[4] Federal Communications Comission, "Twentieth Mobile Wireless Competition Report," 2017.

[5] J. A. Volpe, "VULNERABILITY ASSESSMENT OF THE TRANSPORTATION INFRASTRUCTURE RELYING ON THE GLOBAL POSITIONING SYSTEM," National Transportation Systems Center , 2001.

[6] C. Arthur, "Thousands using GPS jammers on UK roads pose risks, say experts," The Guardian, 13 Feb 2013. [Online]. Available: https://www.theguardian.com/technology/2013/feb/13/gps-jammers-uk-roads-risks. [Accessed 13 Jan 2019].

[7] K. Hill, "Jamming GPS Signals is Illegal, Dangerous, Cheap, and Easy," Gizmodo, 07 July 2017. [Online]. Available: https://gizmodo.com/jamming-gps-signals-is-illegal-dangerous-cheap-and-e-1796778955. [Accessed 23 January 2019].

[8] W. Belamy III, "Are GPS Jamming Incidents a Growing Problem for Aviation?," Avionics International, 31 JAnuary 2017. [Online]. Available: https://www.aviationtoday.com/2017/01/31/are-gps-jamming-incidents-a-growing-problem-for-aviation/. [Accessed 23 January 2019].

[9] J. Capon, "High-resolution frequency-wavenumber spectrum analysis," *Proceedings of the IEEE,* vol. 57, pp. 1408-1518, 1969.

[10] R. O. Schmidt, "Multiple emitter locations and signal parameter estimation," *IEEE Transactions on Antennas and Propagation,* vol. 34, no. 3, pp. 276-280, 1986.

[11] R. Keen, Wireless Direction Finding and Directional Receiption, London, 1927.

[12] S. Sherman and D. Barton, Monopulse Principles and Techniques, 2nd Ed., Artech House, 2011.

[13] B. Van Veek and K. Buckley, "Beamforming: A Versatile Approach to Spatial Filtering," *IEEE ASSP Magazine,* pp. 4-24, April 1988.

[14] B. Boashash, Time-Frequency Analysis and Processing, London: Academic Press, 2016.

[15] R. Roy and T. Kalith, "ESPIRIT - Estimation of signal parameters via rotational invariance techniques," *IEEE Transactions on Accoustics, Speech, and Signal Processing,* vol. 37, pp. 984-995, 1989.

[16] B. Friedlander, in *Classical and Modern Direction-of-Arrial Estimation*, Burlington, MA, Academic Press, 2009, pp. 10-11, 35-37.

[17] H. Cramer, Mathematical Methods of Statistics, Princeton University Press, 1951.

[18] C. Rao, Linear Statistical Inference and its Applications, Wiley, 1965.

[19] P. Q. C. Ly, "Fast and Unambiguous Direction Finding for DigitalRadar Intercept Receivers," The University of Adelaide, Adelaide, 2013.

[20] R. G. Wiley, The Interception and Analysis of Radar Signals, ArtechHouse Radar Library, 2006.

[21] S. E. Lipsky, Microwave Passive Direction Finding, SciTech Publishing, Inc., 2004.

[22] D. Adamy, EW102: A Second Coarse in Electronic Warfare, Artech House Inc., 2004.

[23] B. Friedlander, "Sensitivty Analysis of the Maximum Likelihood Direcion Finding Algorithm," *IEEE Transactions on Aerospace and Electronic Systems,* vol. 26, no. 6, pp. 953-968, 1990.

[24] B. Friedlander, "Sensitivity Analysis of High-resolution Array Processing Algorithms," in *Sixth Multidimensional Signal Processing Workship,* Pacific Grove, 1989.

[25] B. Friedlander, "A Sensitivity Analysis of the MUSIC Algorithm," in *International Conference on Acoustics, Speech, and Signal Processing,* Glasgow, 1989.

[26] Y. Zhao, D. Anagnostou, J. Huang and K. Sohraby, "AoA Based Sensing and Performance Analysis in Cognitive Radio Networks," in *National Wireless Research Collaboration Symposium,* Idaho Falls, 2014.

[27] T. Dhope and D. Simunic, "On the performance of AoA estimation algorithms in cognitive radio networks," in *International Conference on Communication, Information & Computing Technology (ICCICT),* Mumbai, 2012.

[28] Z. Jaafer, S. Goli and A. Elameer, "Performance Analysis of Beam scan, MIN-NORM, Music and Mvdr DOA Estimation Algorithms," in *International Conference on Engineering Technology and their Applications (IICETA),* Al-Najaf, Iraq, 2018.

[29] M. Wax, "On unique localization of multiple sources in passive sensor arrays," *IEEE Transactions Acoust. Speech Singal Prcess.,* vol. 37, no. 7, pp. 996-1000, 1989.

[30] M. Wax and I. Ziskind, "Maximum likelihood locatization of multiple sources by alternating projection," *IEEE Transactions on Acoustics, Speech and Signal Processing,* vol. 36, no. 10, pp. 1553-1560, 1988.

[31] R. H. Mitch, Et Al., "Signal Characteristics of Civil GPS Jammers," GPS World, 1 January 2012. [Online]. Available: https://www.gpsworld.com/gnss-systeminnovation-know-your-enemy-12475/. [Accessed 23 January 2018].

[32] F. Adcock, " Improvements in Means for Determining the Direction of a Distant Source of Electro-magnetic Radiation.". Great Britain Patent GB19180013536 19180820 , 07 August 1919.

REPORT DOCUMENTATION PAGE			Form Approved OMB No. 0704-0188

1. REPORT DATE (DD-MM-YYYY)	2. REPORT TYPE	3. DATES COVERED (From - To)
3-21-19	Master's Thesis	Aug 2016 - March 2019

4. TITLE AND SUBTITLE
Performance Analysis of Angle of Arrival Algorithms Applied to Radiofreqeuncy Direction Finding

5a. CONTRACT NUMBER

5b. GRANT NUMBER

5c. PROGRAM ELEMENT NUMBER

6. AUTHOR(S)
Taylor S Barber, 1Lt

5d. PROJECT NUMBER
FYDJON

5e. TASK NUMBER

5f. WORK UNIT NUMBER

7. PERFORMING ORGANIZATION NAME(S) AND ADDRESS(ES)
Air Force Institute of Technology
Graduate School of Engineering and Management (AFIT/EN)
2950 Hobson Way
Wright-Patterson AFB OH 45433-7765

8. PERFORMING ORGANIZATION REPORT NUMBER
AFIT-ENG-MS-19-M-0087

9. SPONSORING/MONITORING AGENCY NAME(S) AND ADDRESS(ES)
AFRL/RW
Dean Lamonica, 2Lt
203 Eglin Blvd
Eglin AFB, FL,. 32542
dean.lamonica.1@us.af.mil

10. SPONSOR/MONITOR'S ACRONYM(S)
AFRL/RW

11. SPONSOR/MONITOR'S REPORT NUMBER(S)

12. DISTRIBUTION/AVAILABILITY STATEMENT
Distribution Statement A. Approved for Public Release

13. SUPPLEMENTARY NOTES

14. ABSTRACT
Radiofrequency (RF) interference threatens the functionality of systems that increasingly underpin the daily function of modern society. In recent years there have been multiple incidents of intentional RF spectrum denial using terrestrial interference sources. Because RF based systems are used in safety-of-life applications in both military and civilian contexts, there is need for systems that can quickly locate these interference sources. In order to meet this need, the Air Force Research Laboratory Weapons Directorate is sponsoring the following research to support systems that will be able to quickly geolocate RF interferers using passive angle-of-arrival (AoA) estimation to triangulate interference sources.

This research studies the performance of angle-of arrival estimation algorithms for an existing uniform linear antenna array. Four algorithms are studies and algorithm recommendations are made.

15. SUBJECT TERMS
Geolocation, Angle of Arrival, Maximum Likelihood, MUSIC, Beamforming, MVDR, Capon, AOA, AoA, Direction of Arrival, DOA, DoA

16. SECURITY CLASSIFICATION OF:			17. LIMITATION OF ABSTRACT	18. NUMBER OF PAGES	19a. NAME OF RESPONSIBLE PERSON
a. REPORT	b. ABSTRACT	c. THIS PAGE			Dr. Sanjeev Gunawardena, AFIT/ENG
U	U	U	UU	110	19b. TELEPHONE NUMBER (Include area code) sanjeev.gunawardena@afit.edu

Standard Form 298 (Rev. 8/98)
Prescribed by ANSI Std. Z39.18